Abstract

Boothe, Brian J. Goniometric Characteristics of Sapphire Optical Fibers. (Under the direction of Dr. Albert J Shih)

Oblique tip optical fibers are presently used in biomedical applications for the ablation of unhealthy tissue along organ walls. By exploiting total internal reflection at the angled tip, a laser beam guided down the optical fiber exits at an angle perpendicular to the optical axis. The thermal mapping of a developing Diesel after-treatment system requires an accurate knowledge of the wall temperatures within a ceramic filter. Under this research, the same total internal reflection characteristics are examined with respect to accepting versus expelling radiation. Two sapphire optical fibers, one with a flat tip and the other with a 45° oblique tip, were examined. The flat tip fiber was used to validate the experimental configuration while the oblique tip fiber was the focus of this research project. The primary objective was to locate the area from which the oblique tip fiber accepts incident radiation. The flat tip fiber acceptance angle, determined using the angular scan method, was 9°. This was equated to the numerical aperture specifications provided by the manufacturer through the use of an integration method. The oblique fiber accepts a nominal level of radiation from an angle roughly 15° off the central axis with the principal quantity, 10 times greater, accepted from an angle 90° off the central axis through the cylindrical wall. This response is due to the maximum level of total internal reflection off the cut face and minimal wall reflections experienced by the transmitted radiation. The oblique tip fiber experiences an impeded ability to accept radiation when compared to the flat tip optical fiber. In order to receive a similar intensity count on the spectrometer, the integration time was increased from 27 ms to 1200 ms for the flat and oblique tip fibers respectively. This is believed to be a consequence of external reflections due to the cylindrical surface geometry of the fiber. Future research topics are suggested for the oblique tip fiber targeted at isolating the viewing window, increasing the radiation gathering capabilities, and examining the full 360° spatial response.

Goniometric Characteristics of Sapphire Optical Fibers

by
Brian James Boothe

A thesis submitted to the Graduate Faculty of
North Carolina State University
in partial fulfillment of the
requirements for the Degree of
Master of Science

Department of Mechanical and Aerospace Engineering

Raleigh, NC

2002

Approved by:

_____ _____

_____
Chair of Advisory Committee

Biography

Brian J. Boothe is the son of Dr. William L. and Vicky M. Spilker and J. Steven and Diane Boothe. He was married to Marilyn H. Boothe on May 11, 2002, daughter to H. William and Marilyn H. Hull. He has one sister, Jennifer B. Warner.

Brian received a Bachelor of Business Administration in Finance from Southern Methodist University in May 1994 and a Bachelor of Science in Mechanical Engineering from North Carolina State University in December 2001.

Acknowledgments

I would like to thank those professors from the University of Alabama at Birmingham and North Carolina State University who consistently took the time to answer my many questions over the past five years. Of particular note, thanks to Dr. William L. Roberts and Dr. Richard D. Gould for providing guidance and suggestions throughout this research project. Thanks to Dr. Albert J. Shih for encouraging me to attend graduate school, giving me the opportunity to explore this topic, and helping me develop the ideas that made the research a success.

Thanks to Ryan McCall for his graphic contributions to this thesis and to Jian Kong for the pragmatic, often fiery, discussions that helped shape the direction of this project. Special thanks to Robert Hughes who has contributed countless hours to assist in the design and creation of numerous unique, handmade parts during several of my projects, including this research.

I would also like to thank my parents and my parents-in-law for their support during my return to academia. We are all glad the end has arrived.

Finally, and most importantly, I want to thank my wife for her patience and encouragement without which it would have been impossible for me to achieve either degree. We will finally have more time to spend together now that this is over.

Table of Contents

List of Tables

List of Equations

List of Figures

1 Introduction

The extensive use of Diesel engine power is evident in on and off road commercial vehicles as well as land and sea transport. Environmental legislation has encouraged continued research efforts to lower the levels of NO_x and particulate matter emitted by Diesel engines. Research into the development of novel after-treatment filters provides promising solutions in the reduction of harmful exhaust particulates. One such development is a ceramic filter heated by microwaves.

The efficient regeneration of trapped NO_x and particulates requires an accurate knowledge of the temperature distribution within the filter. Traditional thermocouples cannot be employed due to microwave heating and the small cavity structure. An appropriate alternative is the use of single crystal sapphire optical fibers to measure the temperature distribution through infrared radiometry. The material properties of sapphire allow for operation within harsh environments while the optical properties allow transmission of longer wavelength radiation present at relatively low temperatures ranging from 250 to 800°C. Accurate temperature measurement is important to controlling the chemical reactions in Diesel exhaust after-treatment filters.

Precise thermal mapping is achieved by measuring the wall temperatures at various locations within the filter. As shown in the Figure 1.1, traditional optical fibers have polished flat tips accepting incident radiation directly in front of the

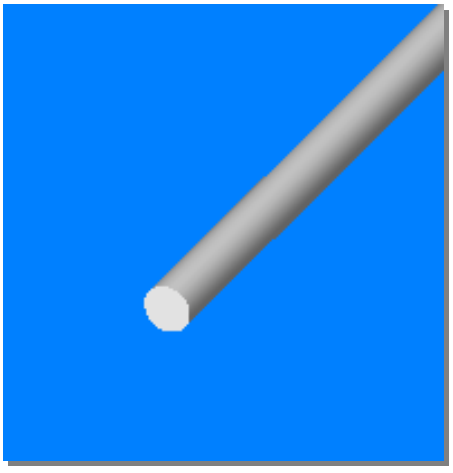

Figure 1.1: Flat tip optical fiber.

fiber through a cone defined by the numerical aperture (NA). The applications of various fiber tip geometries and tip attachments have also been explored to effectively redirect the acceptance region of the fiber [1-9]. One such geometry is the asymmetric oblique tip fiber as shown in the Figure 1.2. The particular geometry used for this research is a 45° beveled tip.

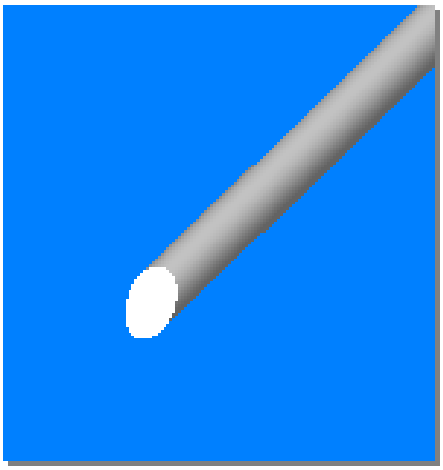

Figure 1.2: Oblique tip optical fiber.

It is necessary to know the exact location along the filter wall from which the fiber accepts incident radiation. Previous research performed in biomedical engineering studied the output of laser light coupled through optical fibers with various tip geometries. The application of side emitting optical fibers for endoscopic operations in ophthalmology and urology allow for tissue ablation along the organ walls without physically redirecting the tip of the fiber [2-5]. Discussion regarding the acceptance of radiation from an external source, however, is not readily available.

This research focuses primarily on the goniometric characteristics of the oblique tip sapphire optical fiber subjected to incident radiation. The intensity distribution as a function of incident angle is measured to accurately define the principal viewing area of the oblique tip optical fiber. Similarly, the angular response obtained from a flat tip optical fiber is measured such that the experimental configuration can be validated for its accuracy. The experimental data obtained from this research is also evaluated with respect to theoretical models of geometric optics.

2 Research Objectives

2.1 Goniometric characteristics

The primary objective of this research program was to determine the goniometric characteristics of a multimode oblique tip sapphire optical fiber. This refers to the specific direction with which the fiber "sees" radiation. It is commonly known that a flat tip optical fiber accepts normally incident radiation through an acceptance cone directed outward from the tip face as shown in Figure 2.1. The size of the acceptance cone is dictated by the optical properties of the fiber, cladding, and immersing material; be it air, water, or any other substance.

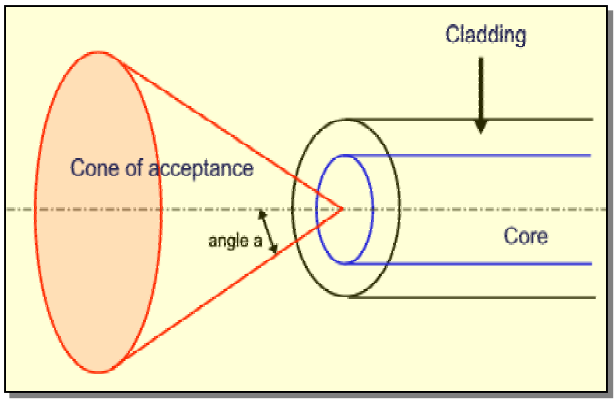

Figure 2.1: Acceptance cone of a typical flat tip optical fiber.

Flat tip fibers cannot be used to determine the temperature of a local spot on the wall of the filter unless the end face is skewed in a direction off the central axis of the fiber. The use of a flat tip optical fiber bent at a 90° angle is inappropriate from a practical standpoint due to the confined spaces within the ceramic filter. An alternative approach is desired spawning exploration into the use of an optical fiber with beveled tip geometry.

It is therefore necessary to know the exact location with which the oblique tip sapphire fiber receives all or most of the environmental radiation. Previously performed theoretical assessments state that the primary source of incident radiation will come from

an area at a small angle off the central axis of the fiber [10,11]. That is, the symmetric distribution experienced by a flat tip fiber would be replaced by an asymmetric distribution. Empirical definition of the asymmetric distribution confirming the theoretical conjecture required this research be conducted.

2.2 Signal intensity

The strength of the signal received by the sensor is also of importance in characterizing the oblique tip sapphire optical fiber. Since the tip geometry is angled at 45°, it is inappropriate to presuppose that the oblique tip fiber will accept a consistent amount of radiation as that of the flat tip fiber. The level of signal intensity will therefore dictate an acceptable distance from the filter wall a fiber may be placed while continuing to receive an accurate directional measurement. It is therefore necessary to quantify the light gathering capability of the oblique tip fiber compared to that of the flat tip fiber.

3 Literature Review

The applications of oblique tip optical fibers have yet to make a significant impression on the engineering community at large. Limited research designed to take advantage of the induced total internal reflection caused by placing an oblique tip optical fiber into substances of various refractive indices to identify chemical compositions has been conducted [12]. Extensive research on the uses of sapphire optical fibers for infrared thermometry has also been performed, however, exploitation of various tip geometries has mainly been isolated to the biomedical engineering field [13,14].

The use of laser "scalpels" in endoscopic surgical procedures has been researched particularity for the ophthalmology and urology fields [2-5]. Traditional flat tip fiber laser endoscopes are constrained to forward firing in tissue removal procedures. The development of apparatuses attached to the distal end of the fiber allowed for redirection of the tip such that tissue along organ walls could be ablated. For microsurgical procedures, the attachments are too large, hindering the removal of tissue around the periphery of the organ. By firing laser light through an optical fiber with beveled tip geometry, the radiation reflects off the angled end surface, exiting at a large angle off the optical axis. Variation in the fiber tip angle dictates the laser exit angle as has been shown by experiment and ray tracing techniques [2,3].

Of particular interest to this research is the response of an optical fiber with 45° angled tip geometry. By firing an argon laser through a 45° oblique tip optical fiber encapsulated within a cylindrical tube of photographic paper, Russo, et al. (1984, 1985) showed that the output beam has a primary and secondary component. The primary component is located perpendicular to the optical axis exiting through meridional surface

while the secondary is roughly 15° off the optical axis in the same direction. A third component, of much less intensity than the first two, was also observed 180° opposite the primary component. This research provided the first visible interpretation of the output characteristics of an oblique tip optical fiber yet gave no definitive reasoning for the regions observed.

It stands to reason that the acceptance of incident radiation will exhibit a similar response experienced when radiation is expelled. This research explores that possibility and attempts to explain the results.

4 Research Methods and Materials

4.1 Experimental model

The first experimental procedure employed to measure the numerical aperture of the sapphire optical fibers was the far-field pattern (FFP) method. This is a widely used method for measuring the acceptance angle of optical fibers [15-17]. The experiments conducted in this research were based largely on instructions defined by the International Electrotechnical Commission (IEC) international standard CEI/IEC 60793-1-43, *Optical fibres – Part 1-43: Measurement methods and test procedures – Numerical aperture* [18]. The IEC standard presents two techniques for measuring the numerical aperture of optical fibers; 1) angular scan, and 2) scan of the spatial field pattern. The angular scan method was chosen as the primary method for this research program. The main deviation from the procedures dictated by the IEC standard is that, in the research method for this thesis, radiation is incident upon the fiber versus being emitted from the fiber. This altered approach was used to measure the angular characteristics of the flat tip fiber at high temperature and the oblique tip fiber at high and low temperature.

In addition to the above approach, a method presented by Photran LLC, the manufacturer of the optical fibers, and adapted from previous research, was also performed [13,19]. The Photran method involves incident radiation upon a variable diameter aperture located in front of the sapphire optical fiber. By varying the diameter of the aperture, the acceptance angle can be measured using trigonometric relationships. This approach was used exclusively to measure the acceptance angle of the flat tip fiber at low temperature.

4.1.1 Angular scan technique

According to the standard procedures presented by the IEC, the angular scan technique for determining the numerical aperture of an optical fiber requires several steps. First, proper alignment must be achieved between the radiation source and the optical fiber. Secondly, both the radiation source and the optical fiber must be properly aligned with the central axis of the rotational stage. This process ensures that the radiation source will consistently point toward the fiber throughout the angular scan method. Furthermore, the rotational stage must be capable of traversing the complete acceptance cone of the optical fiber.

As prescribed by the standard, the 850 nm wavelength was chosen for spectral measurement. This wavelength is most commonly monitored for far-field infrared measurements [18,20]. The radiation scan is then performed and the intensity is recorded as a function of angular position. That is, the intensity received by the sensor is measured as a function of the radiation source angular position relative to the optical axis. The experimental setup, shown in Figure 4.1, has the radiation source rotating about the

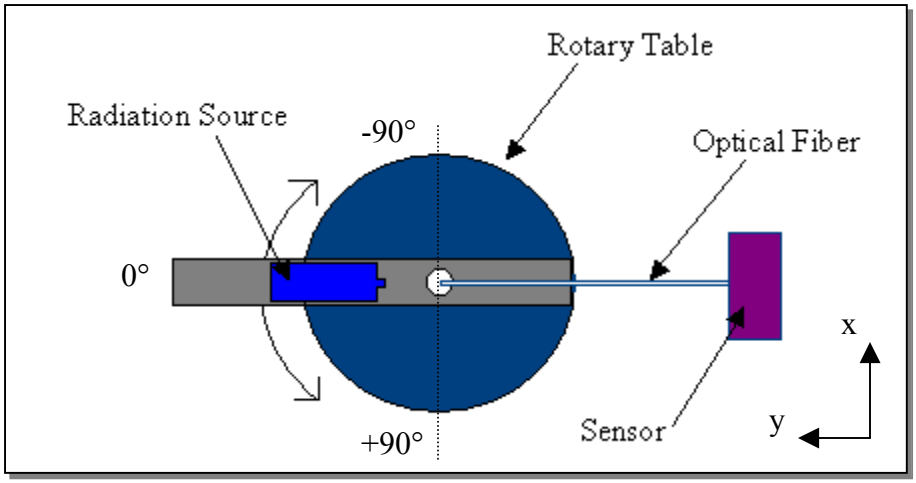

Figure 4.1: Angular scan experimental configuration. (z-axis points out of the page).

table's central axis between angles -90° and +90°. The radiation source is therefore pointing at the fiber tip throughout the full rotation. The zero degree coincides with the optical axis of the fiber.

The intensity is then normalized by the maximum intensity received during the angular scan. The angle at which the intensity measured 5% of the peak intensity is then used to determine the numerical aperture using the following standard equation [18]:

$$NA_{ff} = \sin\theta_{5\%} \tag{4.1}$$

where

NA_{ff} is the far field numerical aperture
$\theta_{5\%}$ is the 5% intensity angle

It has been discovered that the definition of numerical aperture is not consistent among manufactures of optical fibers and the IEC standard procedure. The variable aperture diameter technique, as will be further described in the following section, is another method used to determine the numerical aperture.

In order to equate the two procedures, a numerical integration method is required. The intensity distribution obtained from the angular scan method must therefore be fit to a mathematical curve. For this experimental process, the mathematical software program Maple V, with a least squares curve fit application, was employed to create an equation closely mimicking the actual intensity distribution. The equation was then integrated over prescribed limits and compared to the response provided by the manufacturer.

4.1.2 Variable aperture diameter technique

The variable aperture diameter technique for defining the numerical aperture of an optical fiber was presented by the fiber manufacturer Photran, LLC [19]. Under this approach, the optical fiber is placed a fixed distance behind an aperture as shown in

Figure 4.2. The central axis of the optical fiber and the center of the aperture are aligned. Incident upon the aperture is the source of radiation. The radiation source is placed a distance from the aperture such that the incident radiation is spatially uniform.

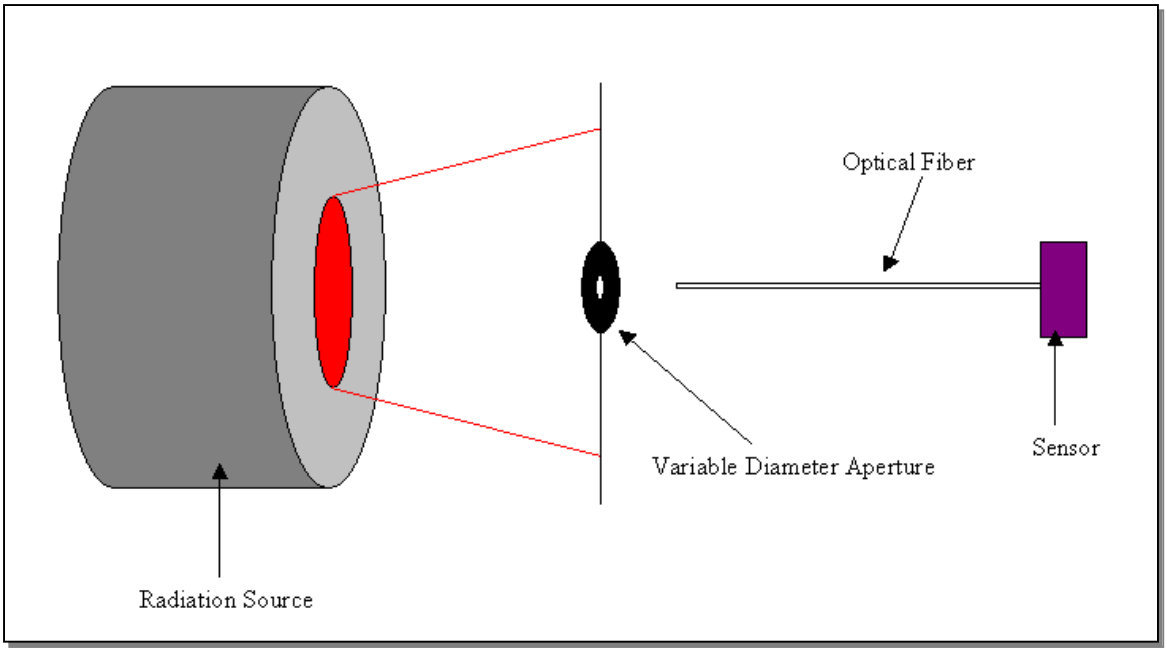

Figure 4.2: Variable aperture diameter experimental configuration.

To quantify the fiber's acceptance angle, a measure of the radiation intensity is taken as a function of increasing aperture diameter. Initially, the intensity level grows exponentially as the diameter of the aperture is increased. Eventually, the increase in aperture diameter no longer causes an exponential increase in intensity and the responses begin to flatten out. At this point, the distribution of incident radiation is greater than the acceptance cone of the optical fiber. As shown in Figure 4.3, by knowing the distance from the aperture to the fiber tip as well as the diameter of the aperture, the acceptance angle, and subsequently the numerical aperture, can be calculated using the following trigonometric relation:

$$\theta = \tan^{-1}\left(\frac{a}{b}\right) \qquad (4.2)$$

$$NA = \sin\theta \qquad (4.3)$$

where

a is half the aperture diameter
b is the distance from the fiber tip to the aperture
θ is the acceptance angle

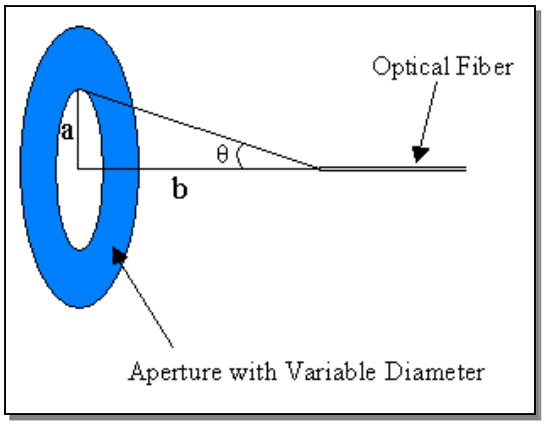

Figure 4.3: Parameters used to define the NA under the variable aperture diameter techniaue.

According to Photran, the numerical aperture of the flat tip optical fiber is 0.10 to 0.12 when this method is implemented [21].

4.2 Experimental materials and applications

The accurate measurement of the goniometric characteristics of both fibers was accomplished through the used of the materials discussed in this section. First, the material and optical properties of the sapphire optical fibers are provided followed by an outline of the rotary table and plank attachment, radiation sources and control systems, micropositioning system, optical cage components, laser alignment system, and photo detection sensors and software.

4.2.1 Flat and oblique tip sapphire optical fiber

Two optical fibers were used for this research project. Both fibers were unclad, multimode, single crystal sapphire (Al_2O_3) with a diameter of 0.425 mm and a length of 1 m. The distal end of the flat and oblique tip fibers was polished at an angle relative to the optical axis of 90° and 45° respectively. The proximal end has an SMA905 connection allowing for efficient coupling of the transmitted radiation directly into the sensor. The

fibers were shielded from the proximal end along 2/3 of the length by a stainless steel flexible armoring.

Sapphire has a melting point of 2040 °C allowing for efficient operation in high temperature environments [22]. Optically, sapphire transmits wavelengths over a range from around 0.45 μm to beyond 3.5 μm. The fiber refractive index is 1.75 and the transmission approaches 85% within the wavelength range measured in this research [21].

4.2.2 Rotary table and plank attachment

According to the angular scan method, a suitable rotational device should be used to encompass the full acceptance cone of the optical fiber [18]. Shown below in Figure 4.4, a 250 mm diameter machinist's rotary table, graduated in 1-minute increments, was used for this experiment allowing for rotation in excess of 180º adequately traversing the angular region in which the optical fiber will accept light. One-minute graduations provide a level of accuracy far greater than that necessary to adequately define the acceptance angle of the optical fiber.

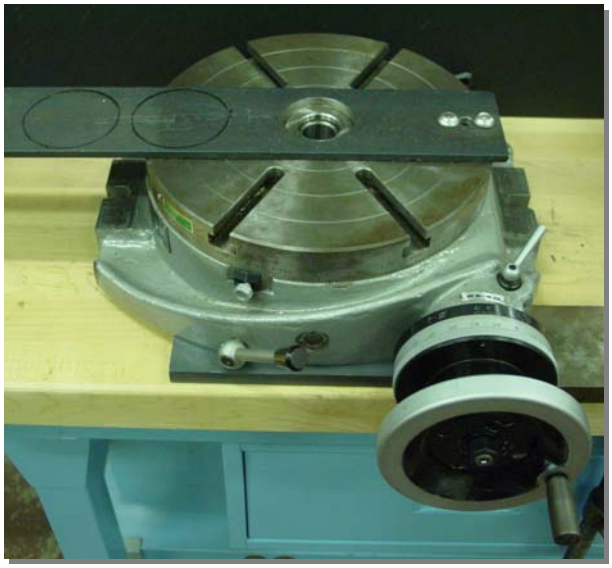

Figure 4.4: Rotary table with plank attachment.

Mounted atop the rotary table, along T-slot grooves on the face, was an extension plank designed to hold the radiation sources at various distances from the central axis.

4.2.3 Radiation source and components

4.2.3.1 High Temperature radiation source

For high temperature measurement purposes, the Ocean Optics LS-1 tungsten halogen light source with a color temperature of 3100 K was used; see Figures 4.5 below. The light output closely resembles the spectral distribution of a blackbody at 3100 K as defined by a Planck distribution. The light is channeled down a set of optical tubes designed to encapsulate the entire spatial output of the LS-1. At the termination of the tubes is a calibrated iris diaphragm with a minimum and maximum diameter of 1 and 12 mm, respectively, graduated in 0.5 mm increments. The iris diaphragm allows for accurate sizing of various aperture diameters such that the radiation spot incident on the optical fiber tip will remain consistent throughout the range of experimental measurements. The optical tubes, iris diaphragm, and LS-1 are held fixed by a precision optical cage assembly mounted on 25 mm posts attached to permanent magnets. The entire assembly was placed on the plank connected to the rotary table.

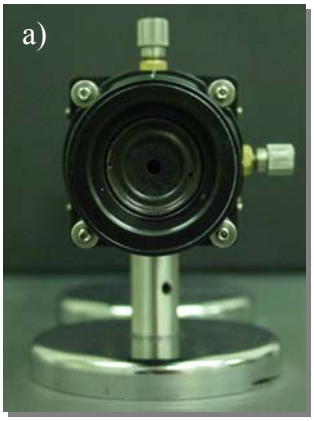

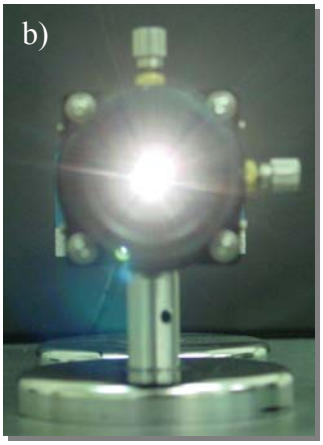

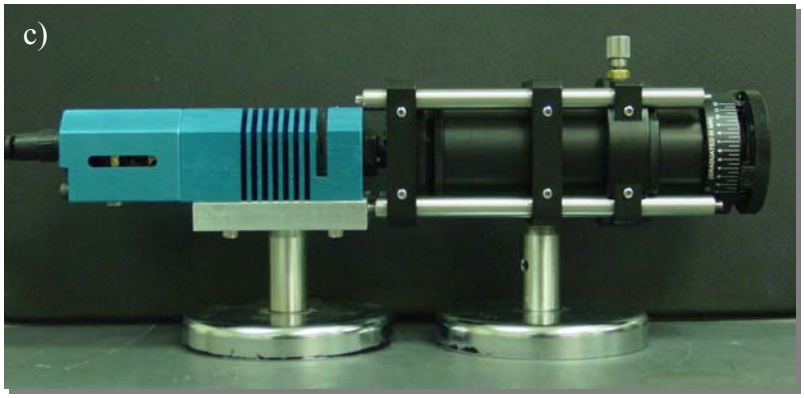

Figure 4.5: High temperature radiation source. a) Front view of precision iris diaphragm, b) front view with light activated, and c) side view of complete radiation source components (LS-1, optical tubes in cage assembly, and precision iris diaphragm).

4.2.3.2 Low Temperature radiation source

An Inconel cavity, prepared such that its characteristic emissivity approaches that of a blackbody, was used as a radiation source for low temperature measurements. Three heavily insulated Inconel tubes were individually controlled with Omega 1/16 DIN CN8201-DC1 PID controllers interfaced through Omega SSR240 DC25 solid-state relays. The controllers allowed for the Inconel cavity to be precisely set to temperatures ranging from 400 to 800 °C. The cavity was affixed to the plank by a series of hose clamps around the circumference. Affixed to the face of the radiation source, a plate with a centrally located 3 mm diameter hole provided an aperture for the low temperature measurements.

Figure 4.6: Blackbody radiation source power, solid-state relay, and controller housing.

Figure 4.7: Omega PID controller used with Inconel blackbody. PV=process value, SV= set value

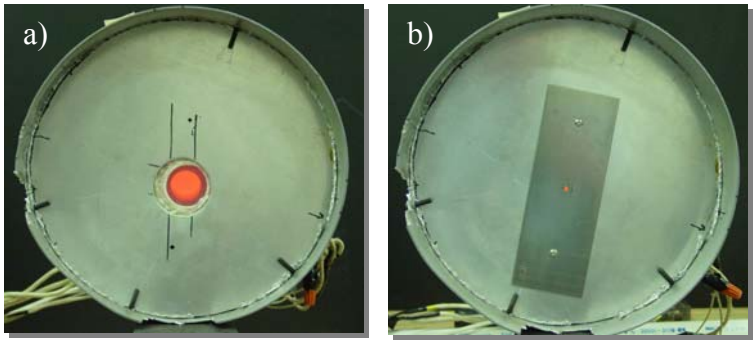

Figure 4.8: Inconel radiation source at operating temperature of 700 °C, a) without 3mm aperture plate attachment and, b) with 3mm aperture plate attachment.

4.2.4 Micropositioning linear translators

Precise positioning of the optical fiber and light source for all experiments was absolutely vital to ensure repeatability throughout the research program. This was achieved, in part, through the use of a three axis micropositioning system. As shown in the Figure 4.9, the coordinate system chosen for this research aligned the *x*-axis horizontally perpendicular to the fiber axis, the *y*-axis parallel to the fiber axis, and the *z*-axis vertically perpendicular to the fiber axis.

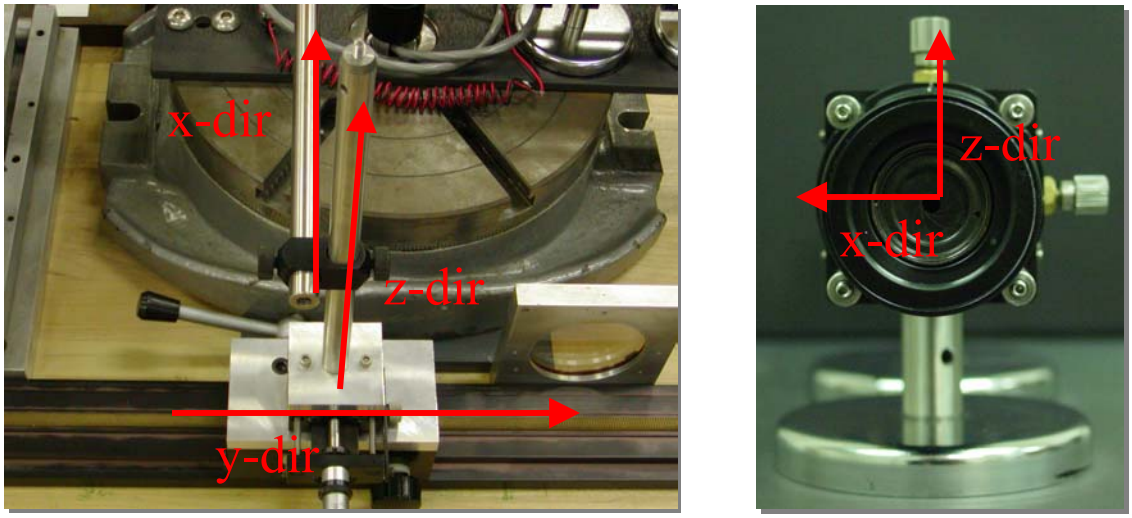

a) b)

Figure 4.9: Coordinate system established on, a) micropositioning linear translator and, b) precision iris diaphragm.

This system required individual linear translators for each direction of motion. A 25 mm travel precision translation stage was mounted atop a 610 mm rack and pinion precision linear slide translator providing motion along the *x* and *y*-axes respectively. Mounted atop the *x* and *y*-axis translators, a vertically oriented 203 mm post with a right angle post clamp affixed a horizontally positioned 203 mm post allowing less precise *x* and *z*-axis motion. To provide further accuracy in positioning, an *x*-*z* translating stage

was mounted directly to the optical cage assembly such that the radiation spot, normally incident on the sapphire fiber tip, would be placed at the location of highest intensity. The *x-z* translator allowed ±1 mm displacement from the center position along both axes.

4.2.5 Mounted optical cage

In performing the low temperature variable diameter acceptance angle experiment on the flat tip optical fiber, it was necessary to mount the optical cage directly to the x-y-z translator as seen in Figure 4.10. The 25 mm posts and permanent magnets were removed from the cage assembly. The cage could therefore be positioned precisely in all directions such that the fiber would be along the central axis as will be discussed in greater detail in a following section.

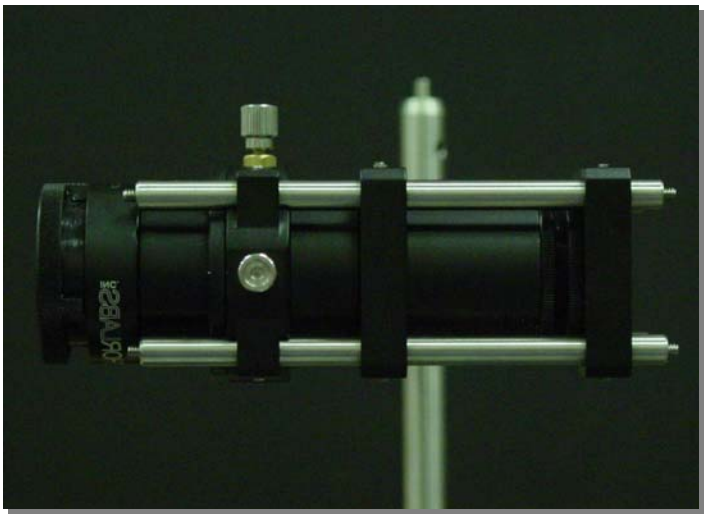

Figure 4.10: Cage assembly with precision iris diaphragm, used to measure the flat tip optical fiber at low temperature.

4.2.6 Laser diode and components

To aid in the fiber alignment procedure, a battery powered 650 nm laser diode with 3.5 mW optical power was mounted concentrically within a custom manufactured support piece shown in Figure 4.11. Press fit along the circumference of the support piece was a

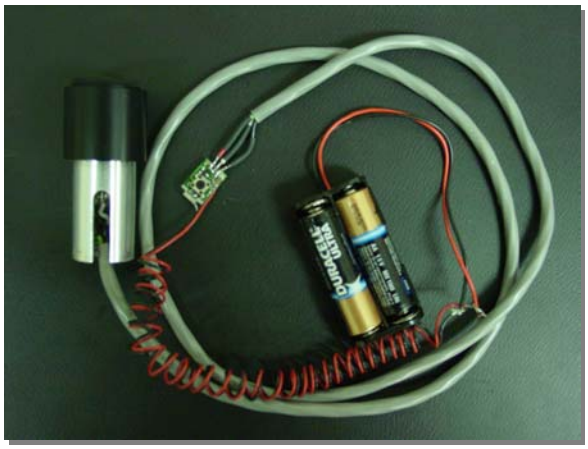

Figure 4.11: Complete laser diode assembly used to align the fiber, table, and radiation source.

25 mm diameter threaded retaining ring. The retaining ring provided a means for attaching a threaded 25 or 51 mm long lens tube containing a 25 mm diameter, 8 mm thick, plano-convex lens located at the distal end. The lens, with an effective focal length of 25 mm and a back focal length of 20 mm, was used to focus the coherent light emitted from the laser diode. The focal point of the laser light could be raised or lowered such that the spot was level with the height of the center of the iris diaphragm. The laser alignment system, shown in Figure 4.12, allowed a visually accurate means of positioning the optical fiber at the vertically and horizontally oriented central axis of the rotary table and radiation sources respectively.

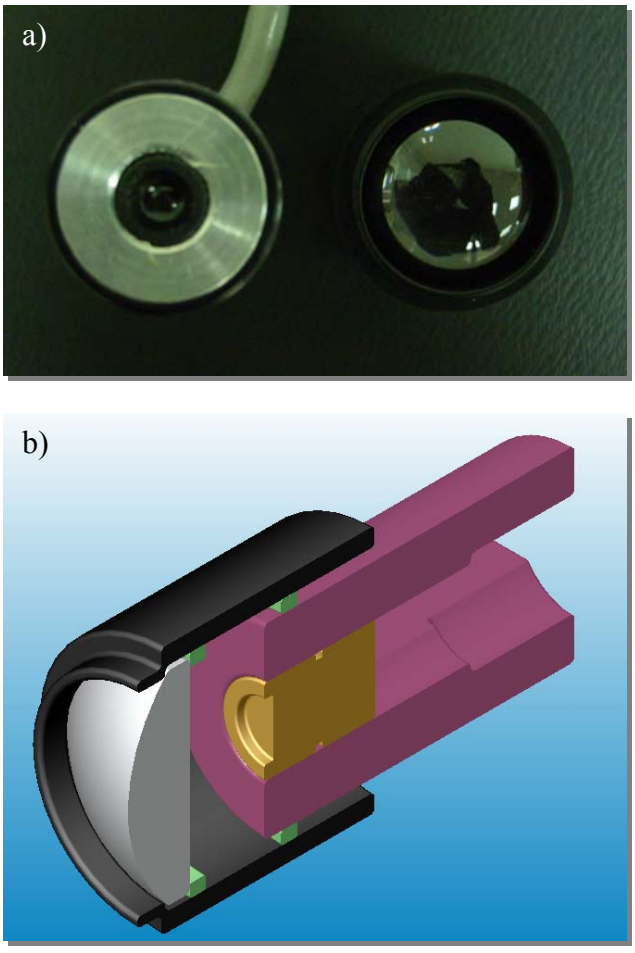

Figure 4.12: a) Top and, b) section views of laser diode and focusing lens system.

4.2.7 Photo detection sensors and software

4.2.7.1 High Temperature sensor

Figure 4.13: USB2000 spectrometer used in high temperature experiments.

For conducting the measurement of accepted incident radiation at high temperature, the Ocean Optics USB2000 miniature fiber optic spectrometer, shown in Figure 4.13, was utilized. The detector is a 2048-element linear silicon CCD array configured specifically to detect radiation within the wavelength range of 720 nm to 980 nm. This wavelength span is consistent with the spectral distribution from the Ocean Optics LS-1 tungsten halogen light source at 3100 K. The spectrometer has an estimated sensitivity of 86 photons/count with a signal to noise ration of 250:1. The optical fiber is coupled to the spectrometer through an SMA connection.

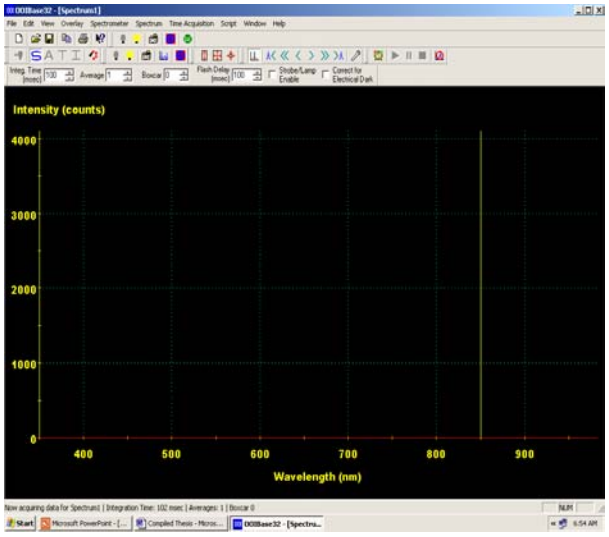

Figure 4.14: Screen output from USB2000 spectrometer software.

The spectrometer is controlled by the Ocean Optics OOIBase32 spectrometer operating software version 2.0.0.3. The package allows the user to vary integration time, spectral averaging, and specific wavelength monitoring. For this research, the data acquisition application was used to monitor the

variation in intensity through a given angular region. A graphical representation of the output response is also written to the screen shown in Figure 4.14.

4.2.7.2 Low Temperature

At lower temperatures, the wavelength of the emitted radiation becomes longer. According to the Wien displacement law, the peak wavelength for temperatures 400 and 800 °C are 4.3 and 2.7 μm respectively, versus 0.97 μm for 3100 K [23]. These wavelengths are certainly outside the range of the USB2000 spectrometer. It was therefore necessary to use a Lead Sulfide (PbS) photoconductor, shown in Figure 4.15, manufactured by Electro-Optical Systems, Inc., with an operating wavelength in the range of 1 to 2.8 μm, peaking at 2.5 μm. The sensor is connected to a PS/TC-1 TEC Power Supply/Controller also manufactures by EOS. Since the input signal from the radiation

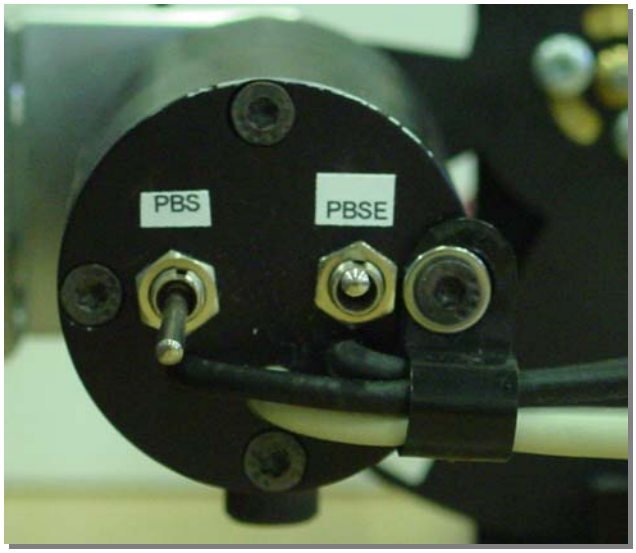

Figure 4.15: Lead Sulfide (PbS) sensor used in low temperature experiments (PbSe was not used for this research).

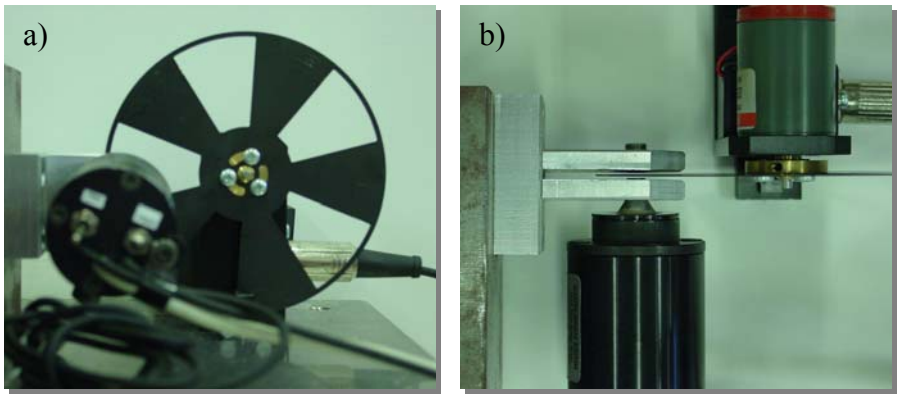

Figure 4.16: Chopper system from, a) side view and, b) top view.

source is DC and the photoconductive sensor requires an AC input, the signal had to be "chopped" to create a wave function. This was accomplished through the use of the Model 300CD five-blade optical chopper system, shown in Figure 4.16, supplied by Scitec Instruments LTD. The chopping frequency was set to 250 Hz (±10 Hz) for the optimum signal to noise ratio as dictated by the sensor manufacturer.

The sensor output is an alternating voltage originally measured using an HP 54645A oscilloscope. To aid in the data acquisition process, the National Instruments LabVIEW 6i single channel oscilloscope virtual instrument, shown in Figure 4.17, in conjunction with the National Instruments MIO-16E Series DAQ, was used to measure the peak-to-peak voltage from the PbS sensor with the output recorded in a spreadsheet application. By using the LabVIEW application, exact values of peak-to-peak voltage could be measured at very low relative levels of voltage response.

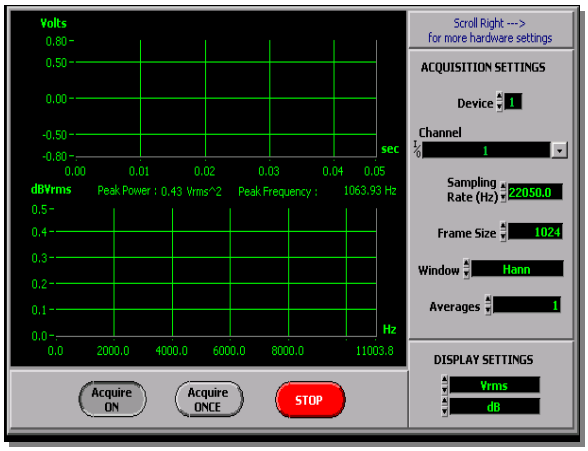

Figure 4.17: Screen output from LabVIEW oscilloscope virtual instrument.

4.3 Alignment procedures

As stated previously, precise alignment of the various components utilized in this research was paramount in achieving accurate, reproducible results. The following section details the extensive measures executed in aligning the laser diode, optical fiber, and radiation source to ensure such an outcome.

4.3.1 Laser diode alignment

The custom support piece, created to hold the laser diode and mount the focusing lens, was placed along the central *z*-axis, pointing in the vertically upward direction. A target grid, attached to a post assembly and mounted external to the rotary table, was placed directly above that lens at the distance corresponding to the known focal point. This created a small focused spot on the target grid that could be monitored as the rotary table was in motion. The rotary table was then revolved through 180° while the location of the spot was tracked as shown in Figure 4.18. The rotary table was then returned to the original position and the spot was repositioned to the center of the distance made by marking the spot location at 180° relative to the starting position. The target grid was then repositioned such that the accurate point of origin could be monitored and the process was repeated. To ensure the laser support piece remained in place, a shim was attached along its circumference to create a tight friction hold between the piece and the through hole wall in the center of the rotary table. When the spot remained in the same

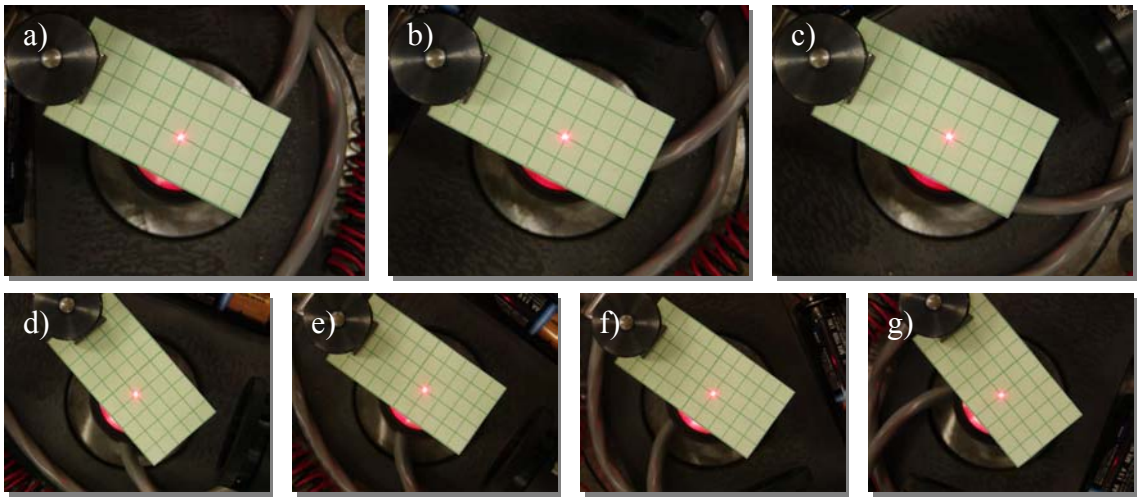

Figure 4.18: Laser diode and focusing lens alignment at, a) -90°, b) -60°, c) -30°, d) 0°, e) +30°, f) +60°, and g) +90°.

location through the 180° rotation, the laser was determined appropriately centered on the rotary table and the process was terminated. As verification that the laser remained centered on the rotary table during all experiments, the alignment process was repeated at consistent intervals throughout this research. It is estimated that the "wobble" of the laser spot when rotated 180°, is significantly less than 0.5 mm. The above Figure 4.18 shows the resulting centered spot location at 30° intervals of 180° rotation from -90° to +90°.

4.3.2 Optical fiber

Consistent alignment of the optical fiber was facilitated primarily through the use of a grooved fiber clamp supplied by Thorlabs, Inc. shown in Figure 4.19. The groove was specifically designed to hold a 425 μm optical fiber. The clamp was mounted directly to the *x*-*y*-*z*-axis translator allowing for the micropositioning of the optical fiber as previously discussed. Initially, the mounted fiber clamp was placed flush along side a machined square block taller than the height of the light source such that the clamp face would be

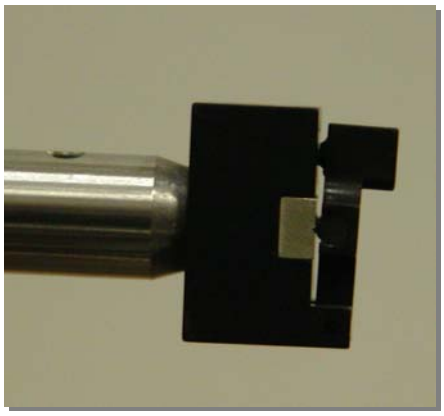

Figure 4.19: Fiber clamp grooved to fit 0.425 mm optical fiber.

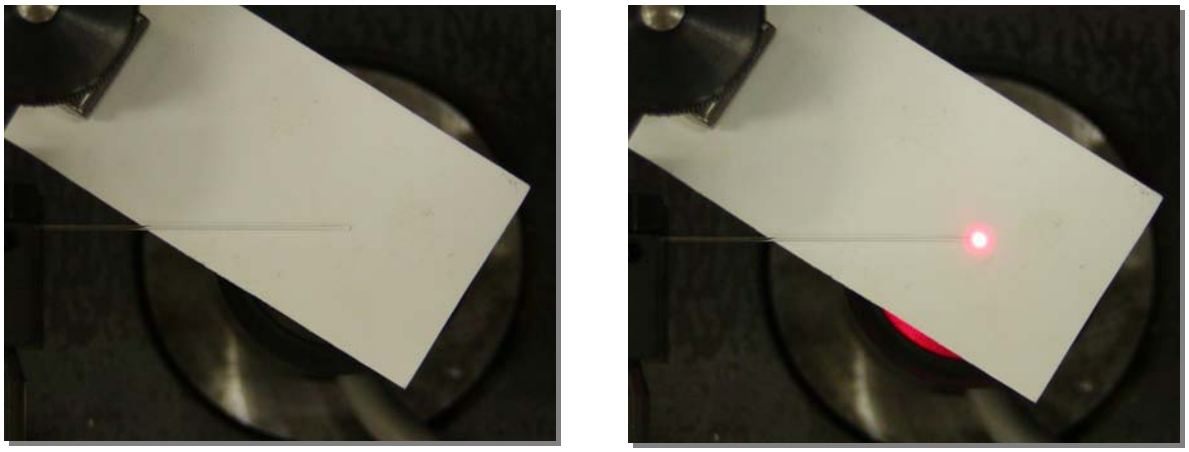

Figure 4.20: Alignment of optical fiber on rotary table with the laser diode.

precisely perpendicular to the surface of the rotary table. This ensured that the central axis of the optical fiber would be normal to the central axis of the rotary table. With the laser diode activated, the optical fiber was moved into position such that the tip of the fiber was centered at the middle of the focal spot output from the lens. This alignment procedure was effective in centering both the flat tip and oblique tip fibers on the rotary table with the previously mentioned error of less that 0.5 mm. A white piece of plastic, shown on the previous page in Figure 4.20, transparent to the emitted light from the laser diode, was placed directly underneath the fiber tip to assist in the alignment process. This alignment procedure was employed for both high and low temperature experiments. The single difference between the two experiments was the use of a 25.4 mm versus a 50.8 mm optical tube lens mount for the high and low temperature experiments respectively. This was due to the difference in height of the two radiation sources.

The second alignment issue concerning the oblique tip optical fiber was the angular position of the cut face relative to the optical axis. To measure the various angular responses, the oblique tip fiber must be manually rotated about the central fiber axis such that the cut face could be oriented at 0°, 90°, and 180°. At the 0° orientation, the cut face was pointing directly downward.

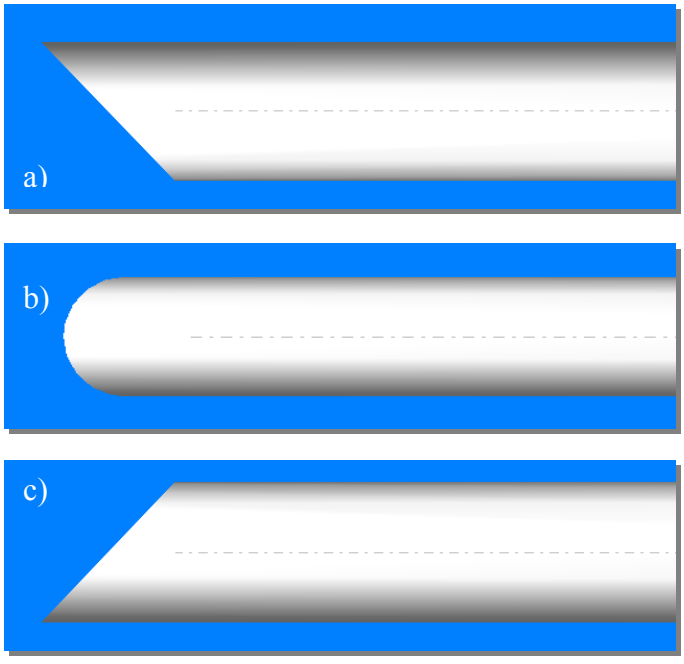

Figure 4.21: Oblique tip fiber orientations, a) 0°, b) 90°, c) 180°.

Facing the fiber and rotating it about the optical axis in a clockwise direction, the 90° and 180° orientations are subsequently achieved. Figure 4.21 shows the various orientations of the fiber relative to the fiber axis.

Alignment of the fiber in the 0° and 180° orientation was facilitated through the use of the laser diode. When the laser light is incident on the cut face precisely at 0°, a spot is reflected along the optical axis in front of the fiber. Using a white piece of plastic, the visible spot is a guide to aligning the fiber into the correct orientation. Conversely, at 180° the laser light reflects off the cut tip face propagating a beam of light directly down the optical fiber emitting a spot from the proximal end. Visually, or with the use of the spectrometer, the greatest intensity of laser light passing through the fiber can be approximated as the orientation corresponding to the fiber at 180°; the cut face situated directly upward.

In a method similar to the 180° alignment procedure, the radiation source is placed at the +90° position on the rotary table. When the optical fiber is rotated into the 90° orientation relative to the optical axis, the largest amount of radiation reflects off the cut face traveling down the fiber. Using the spectrometer to monitor the level of intensity, the highest value is again approximated as the correct 90° orientation. In all circumstances, 0°, 90°, and 180°, the greatest level of accuracy is visually estimated at ±15° off the desired orientation.

4.3.3 Radiation source

The following section identifies the procedures taken to align the radiation source with the optical axis for both high and low temperature experiments.

4.3.3.1 High Temperature

Alignment of the high temperature radiation source was achieved in part with the positioning of the fiber clamp. By shining the light directly toward the fiber clamp face, the incident spot could be roughly centered on the optical fiber through *x* and *z* translation of the post mounting system as seen in Figure 4.22. Through micropositioning the *x*-*z* translator attached to the optical cage system, in conjunction with the spectrometer output profile, the maximum intensity could be optimized thereby locating the center of the radiation source. The light source was subsequently aligned with the optical axis of the fiber. This procedure was used for the alignment of both the flat and oblique tip optical fibers in the angular scan experiments. In accordance with the previously discussed alignment procedures, the fiber was therefore, 1) centered on the rotary table and, 2) centered on the radiation source allowing for accurate, repeatable measurements to be obtained.

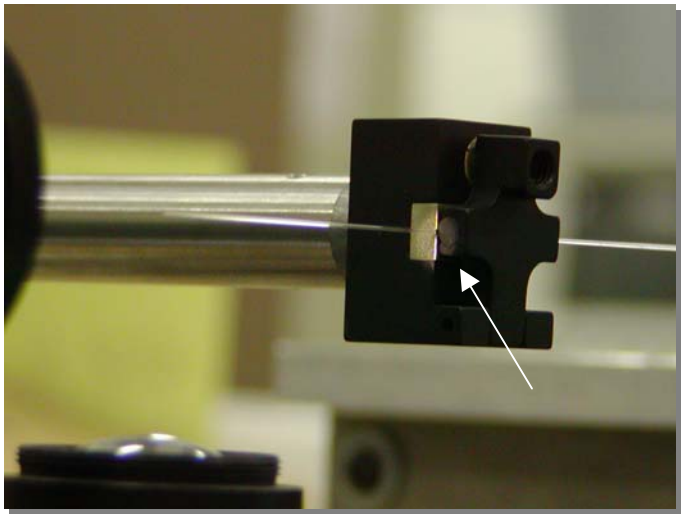

Figure 4.22: Photo of the spot incident on the fiber clamp. The first step in aligning the radiation source with the optical fiber.

4.3.3.2 Low Temperature

For the low temperature angular scan experiment performed on the oblique tip fiber, the procedure outlined at high temperature was also executed. The main variation was that the position of the aperture could not be finely adjusted due to the heat of the blackbody precluding the use of the mounted cage assembly *x*-*z* translator. In this

circumstance, the fiber clamp was repositioned to a higher location along the 203 mm post mount. Again, the spectrometer was utilized to determine the highest value of intensity, thereby marking correct fiber positioning.

As for the flat tip fiber, the variable aperture diameter experiment had to be performed. The optical fiber was placed along the central axis of the optical cage system with the precision variable aperture diaphragm located at the end facing the radiation source. By reducing the diameter of the iris to 0.5 mm, the incident radiation emitted from the blackbody could only be detected if the fiber was exactly located along the central axis of the optical cage system as shown in Figure 4.23. The centered fiber position was obtained by adjusting the *x*-axis micropositioner along with gradually raising or lowering the lab jack on which the fiber rested. Using the oscilloscope, the maximum value of peak-to-peak voltage was found as a consequence of minute position changes and determined to be the most centrally located position of the optical fiber. For this experiment, it was not necessary to align the optical fiber on the rotary table therefore the laser and lens system were eliminated from the procedure.

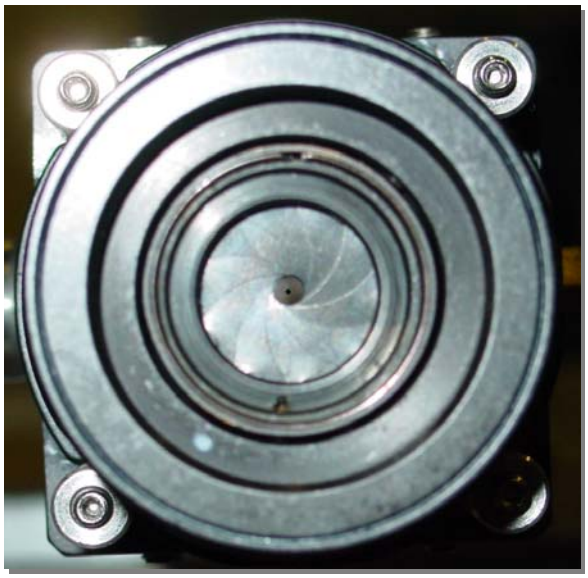

Figure 4.23: Optical cage assembly with fiber positioned along the central axis.

5 Experimental Results

The following section discusses the process performed to determine the numerical aperture and subsequent acceptance angle of the flat tip and oblique tip sapphire optical fibers. Measurements were made at high and low temperatures using the angular scan and variable aperture diameter methods. The resultant data is presented for each experiment conducted.

5.1 High temperature measurements

Since the high temperature experimental procedure afforded a greater level of accuracy during data collection, the following results provide a detailed account of the response obtained from the flat and oblique tip optical fibers. For both fibers, the angular scan method was performed.

5.1.1 Flat tip fiber

By confirming the acceptance angle of the flat tip optical fiber with the angular scan method, validation of the constructed experimental design and alignment methods could be achieved. According to the fiber manufacturer, the numerical aperture should be 0.10 to 0.12 corresponding to an acceptance angle roughly between 6° and 7°. To adequately cover the complete acceptance angle region, a 30° sweep was made at half-degree increments starting at -15° and advancing to +15°. Half-degree increments were determined to be within an adequate level of precision relative to the greater than 1° error presented by the manufacturer. The center of the optical axis was estimated to be within an error of ±1° off the assumed 0° position. Since the output was known to be

symmetric, the point of highest intensity was concluded to be the center of the optical axis.

All high temperature measurements were taken using the Ocean Optics spectrometer. In order to receive accurate data output, the software package requires that the integration time be set such that the intensity count reads approximately 3500 on the screen output. The integration time was subsequently set to 27 ms. To smooth out the noise, the averaging value was set to 30. This corresponds with a spectral output every 0.81 s; (27 ms/sample · 30 samples). Based on the instructions dictated by the IEC standard, the monitored wavelength was 850 nm.

At least ten spectral readings were taken for each degree increment. The resultant ten values were then averaged to obtain a single value for the intensity at each particular degree. The highest value of intensity was then used to normalize the complete angular response into a relative intensity. These values were then plotted as a function of the prescribed angle of measurement. As stated previously, the highest value of relative intensity was then considered to be the center of the optical axis.

To validate the independence of aperture size and the acceptance angle in an angular scan test, the response was measured at an iris diameter of 1 mm and 3 mm. Each test was performed twice with two runs performed per test.

Since the definition of numerical aperture as prescribed by Photran is not directly analogous to that defined by the IEC standard, it was necessary to match curve fit data to the results obtained experimentally such that the area under the response curve could be integrated. This was accomplished through the use of a least squares curve fit function

within Maple V software. By creating a 10^{th} order polynomial, an equation closely simulating the actual angular response was formulated.

5.1.1.1 Test #1; experimental results

The following charts (Figures 5.1 and 5.2) show the actual and curve fit data obtained from Test #1 performed with the iris diameter set to 1 mm and 3 mm independently.

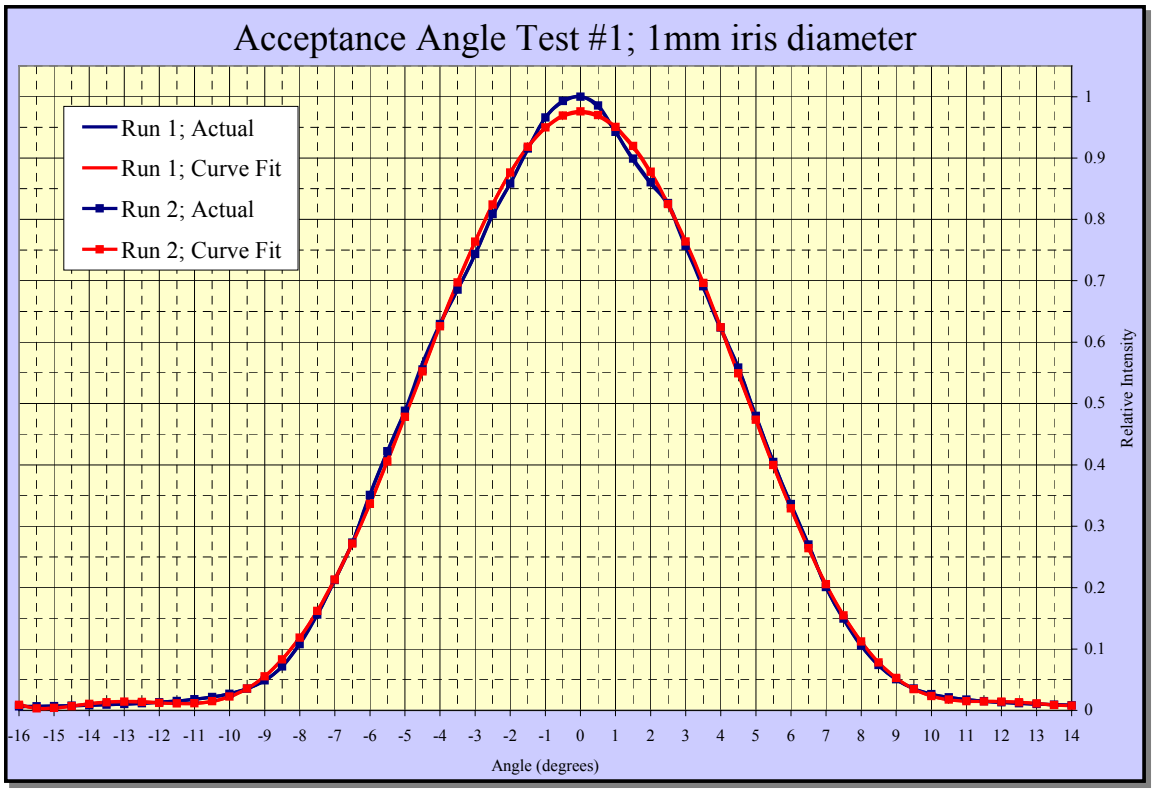

Figure 5.1: High temperature flat tip acceptance angle Test #1 with iris set to 1 mm.

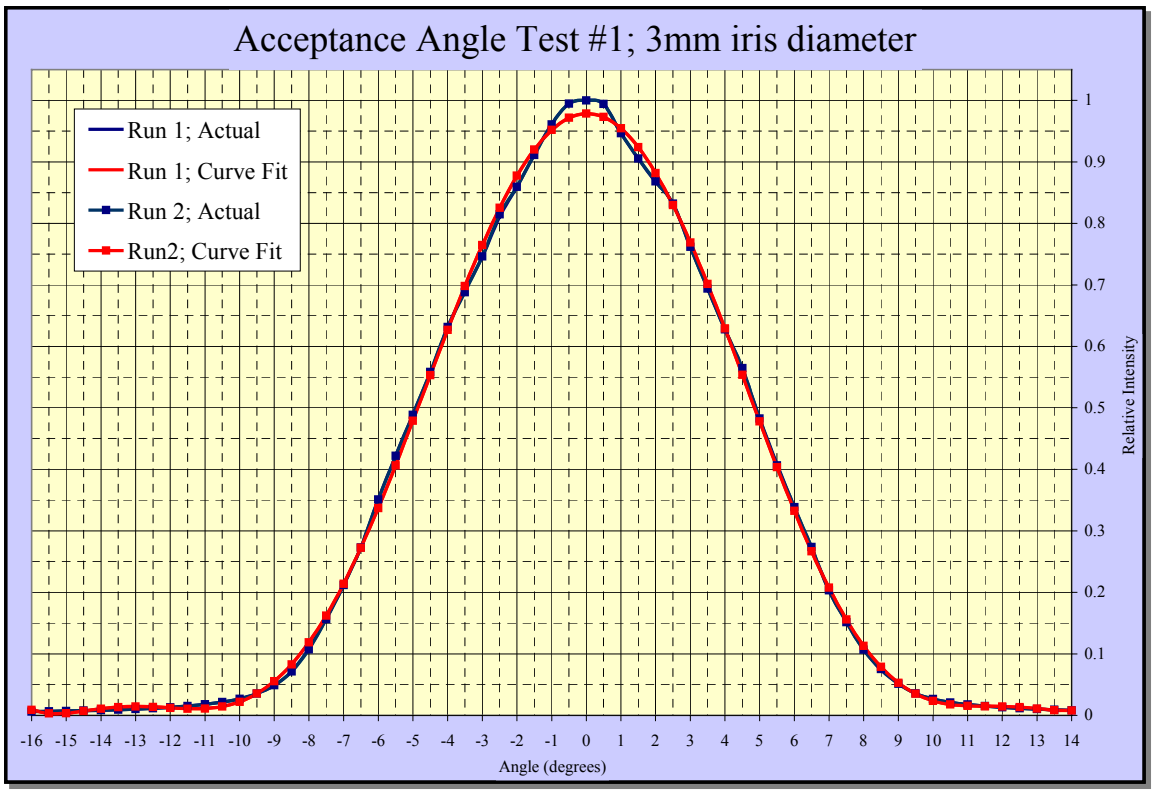

Figure 5.2: High temperature flat tip acceptance angle Test #1 with iris set to 3 mm.

When integrated according to the limits defined by the full curve (-16° → 14°), -6° → +6°, and -7° → +7°, the least squares curve fit equation resulted in the following data table.

Table 5.1: Tabulated percentage of intensity contained under the entire curve and within the 6° and 7° half-angle cones; Test #1.

Numerical Integration of Response Curve; 1mm iris diameter					
	Full Curve	±6°	Percentage	±7°	Percentage
Run 1	19.840	17.415	87.8%	18.492	93.2%
Run 2	19.857	17.431	87.8%	18.507	93.2%
Numerical Integration of Response Curve; 3mm iris diameter					
	Full Curve	±6°	Percentage	±7°	Percentage
Run 1	19.935	17.496	87.8%	18.492	92.8%
Run 2	19.938	17.499	87.8%	18.581	93.2%

The percentage value quantifies the relative level of integrated intensity present within the acceptance cone of half-angle 6° and 7°.

5.1.1.2 Test #2; experimental results

The following charts (Figures 5.3 and 5.4) show the actual and curve fit data obtained from Test #2 performed with the iris diameter set to 1mm and 3mm independently.

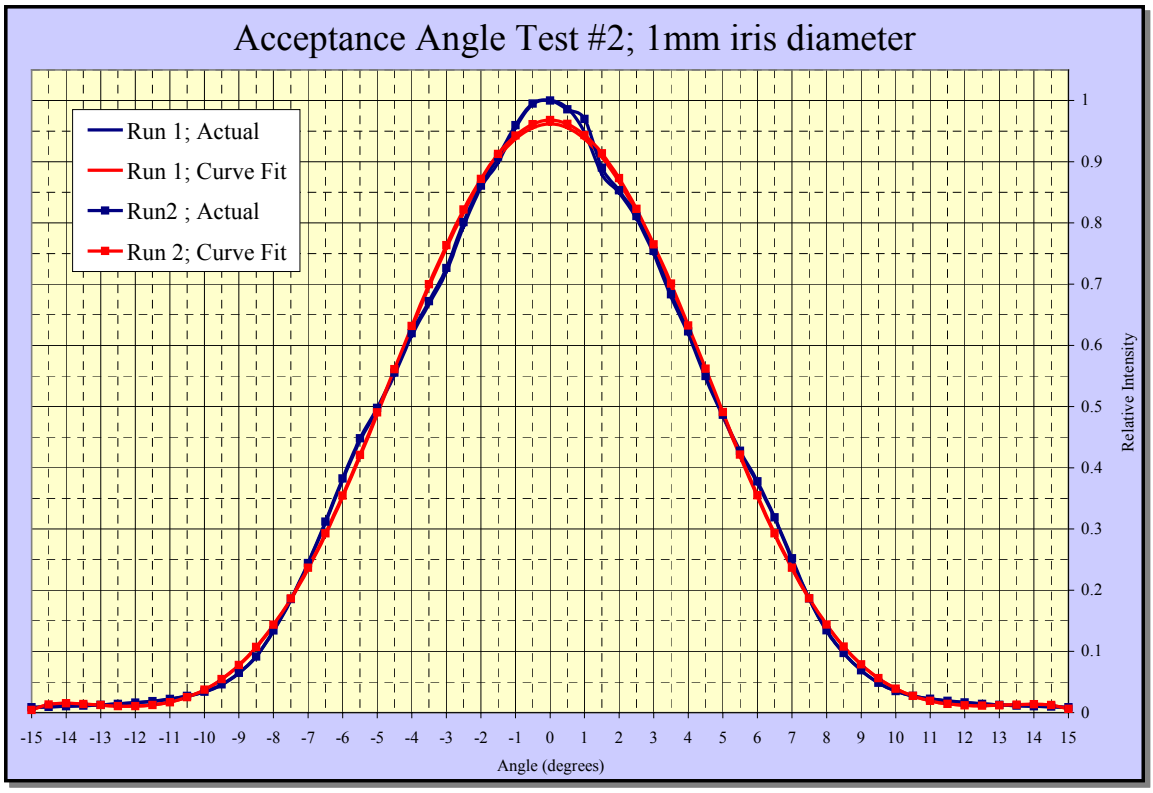

Figure 5.3: High temperature flat tip acceptance angle Test #2 with iris set to 1 mm.

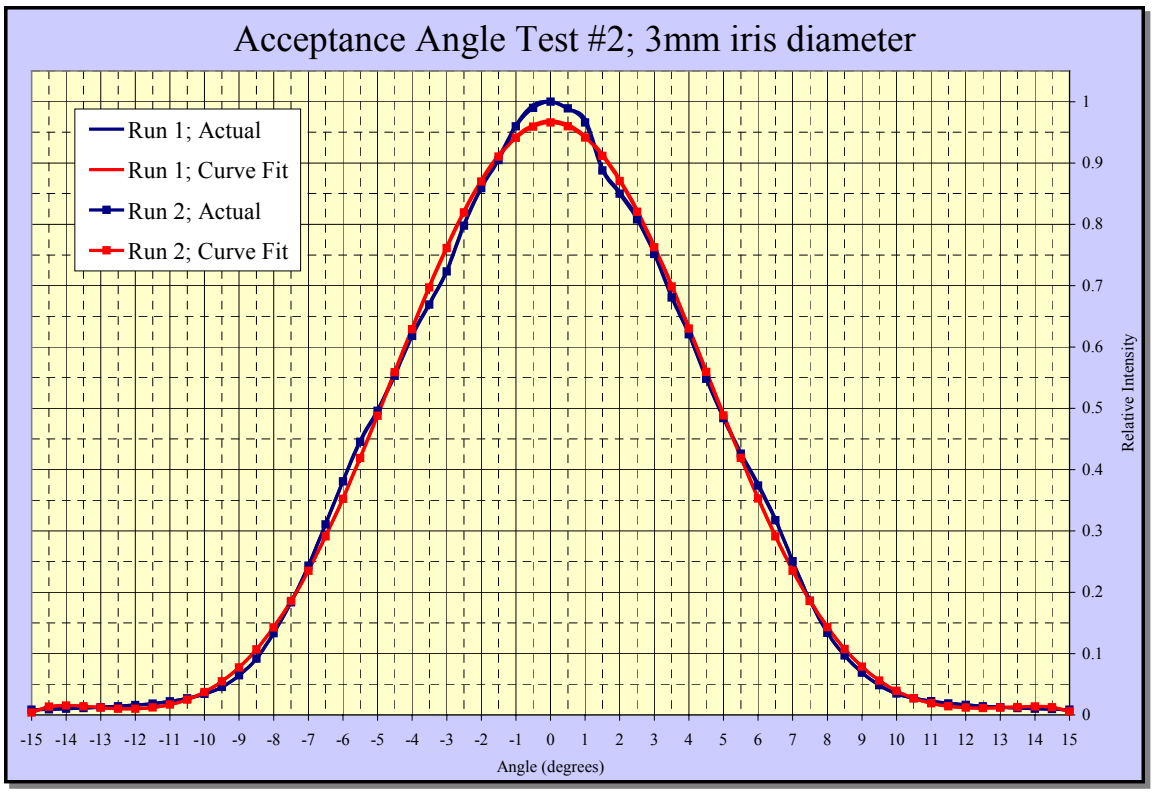

Figure 5.4: High temperature flat tip acceptance angle Test #2 with iris set to 3 mm.

Integrating the least squares curve fit over the same limits as in Test #1 produces the following data table.

Table 5.2: Tabulated percentage of intensity contained under the entire curve and within the 6° and 7° half-angle cones; Test #2.

Numerical Integration of Response Curve; 1mm iris diameter					
	Full Curve	±6°	Percentage	±7°	Percentage
Run 1	20.260	17.389	85.8%	18.554	91.6%
Run 2	19.938	17.499	87.6%	18.581	93.1%
Numerical Integration of Response Curve; 3mm iris diameter					
	Full Curve	±6°	Percentage	±7°	Percentage
Run 1	20.389	17.500	85.8%	18.673	91.6%
Run 2	20.324	17.443	85.8%	18.611	91.6%

5.1.2 Oblique tip fiber

Since little was known about the true response of the oblique tip fiber, it was necessary to measure the characteristics over a full 180° region. Therefore, the radiation source was placed perpendicular to the optical axis (in the -90° position relative to the central axis of the rotary table) with the fiber oriented such that the cut face pointed toward the radiation source (in the 90° orientation relative to the optical axis). Intensity measurements were taken in 5° increments. For this experiment, the aperture diameter was set to 3 mm with no adjustment made on additional experiments.

As before, the spectrometer was configured such that the intensity count read a maximum near 3500 at 850 nm. This required the integration be set to a value of 1200 ms; almost 45 times longer than the flat tip fiber. The averaging was set to 1 due to the relatively large integration time.

In accordance with the flat tip measurements, at least ten readings were taken for each degree increment. The average of the ten values was normalized by the maximum value of the total response then plotted as a function of rotational angle. In this case, the optical axis could not be assumed to be the location of highest intensity as done with the flat tip fiber. It was therefore assumed that the central axis coincided roughly with the location determined under the flat tip fiber experiments; with an error of ±1°.

Based on the response observed from the oblique tip fiber, the peaks and valleys observed were then evaluated on much smaller increments. The hump, valley, and peak, as termed for this report, were defined by measurements made at 30, 20, and 20 minute increments, respectively. This provided more detailed information as to the precise angular response of the oblique tip fiber.

5.1.2.1 90° orientation; Test #1; experimental results

The following chart (Figure 5.5) shows the response obtained from Test #1 with the fiber in the 90° orientation relative to the optical axis. The iris diameter was set to 3mm. It was necessary to extend the angular scan from 180° to 235° such that the complete response could be measured.

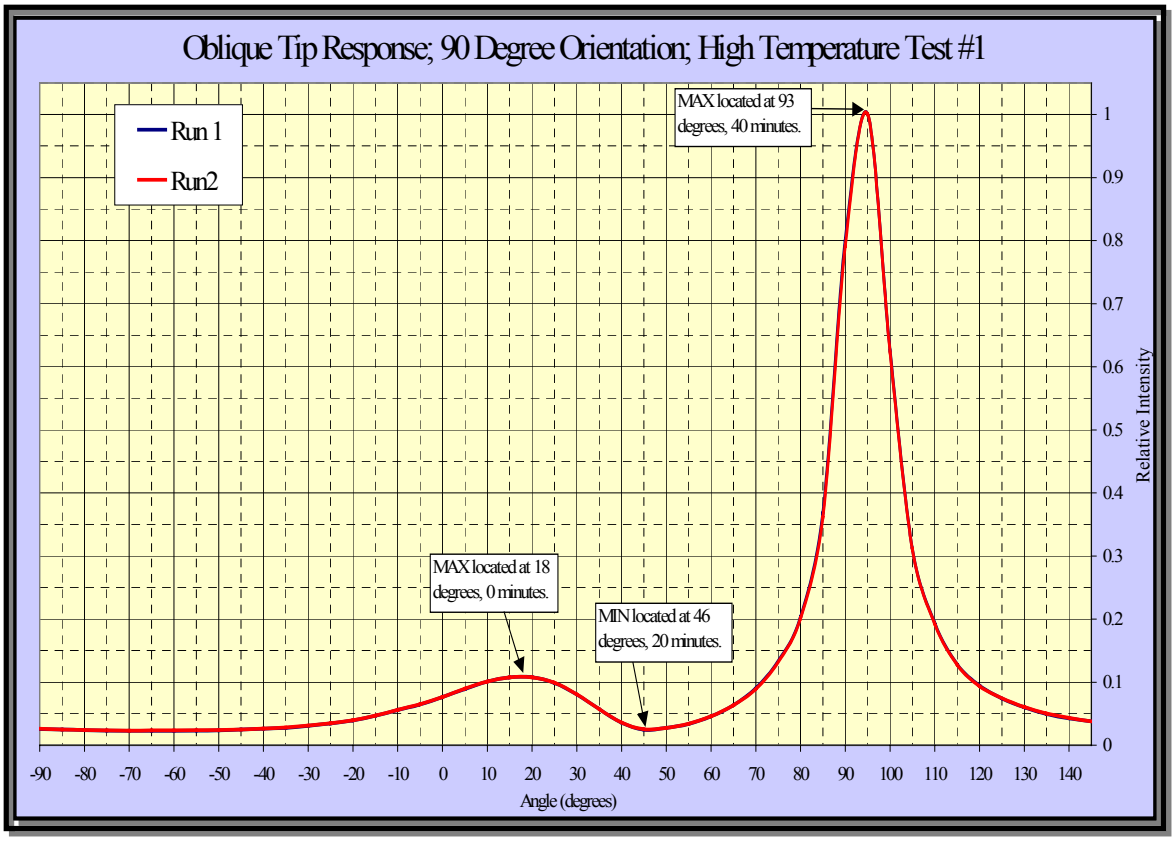

Figure 5.5: High temperature oblique tip intensity profile with fiber in the 90° orientation; Test #1.

5.1.2.2 90° orientation; Test #2; experimental results

The following chart (Figure 5.6) shows the response obtained from Test #2 with the fiber in the 90° orientation relative to the optical axis. The iris diameter was set to 3mm.

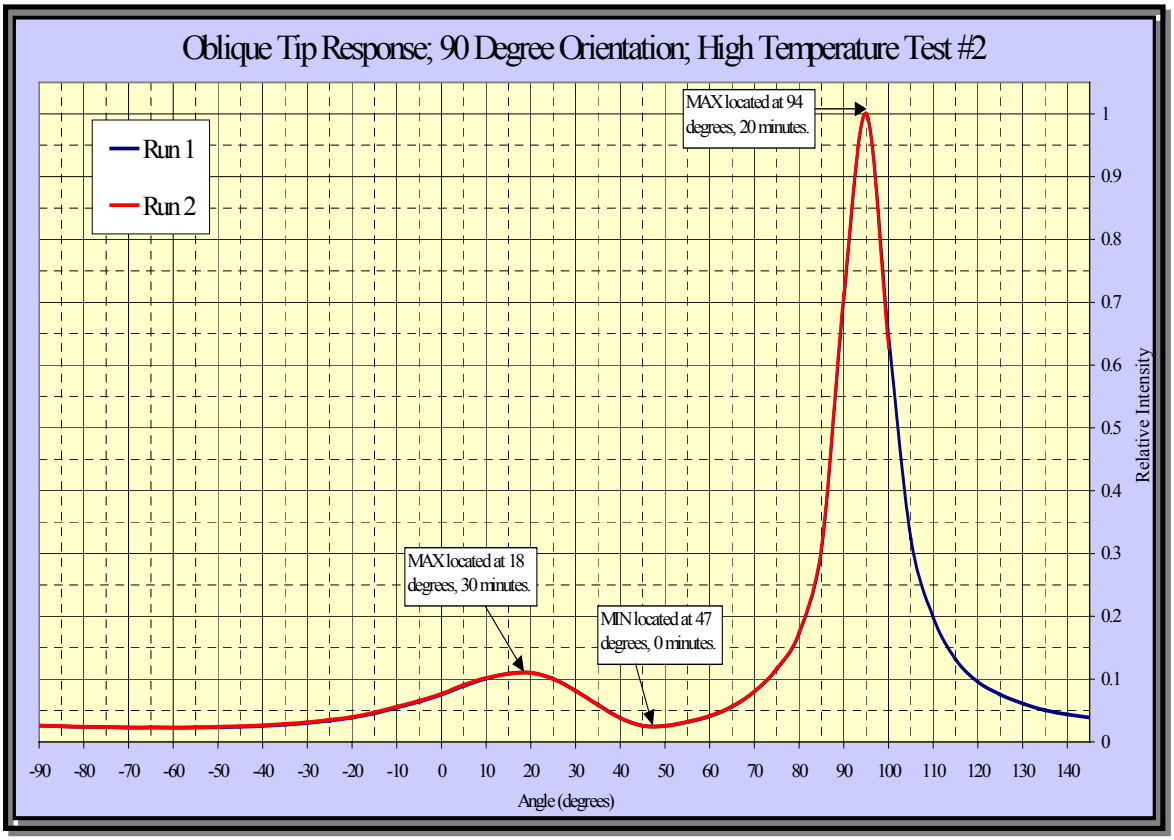

Figure 5.6: High temperature oblique tip intensity profile with fiber in the 90° orientation; Test #2.

5.1.2.3 0° orientation; experimental results

The following chart (Figure 5.7) shows the response obtained from the experiment performed with the fiber in the 0° orientation relative to the optical axis. The iris was set to 3mm.

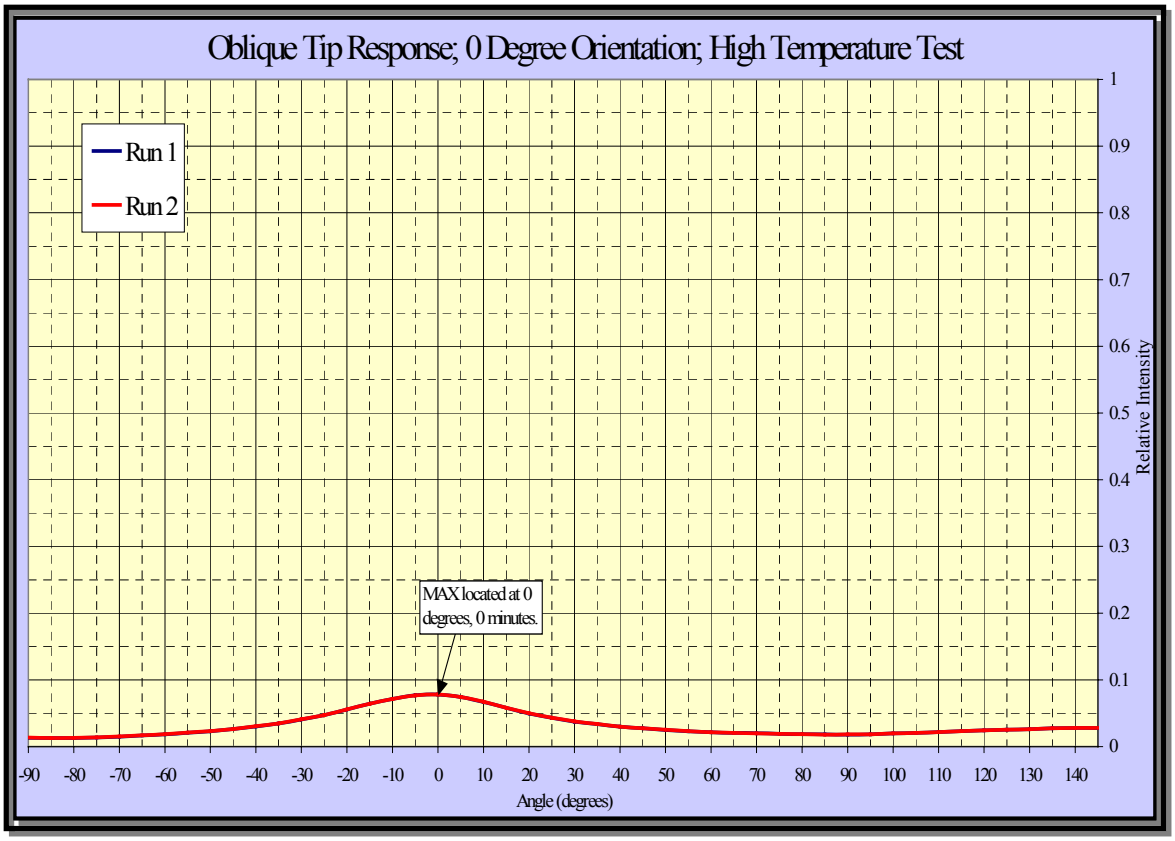

Figure 5.7: High temperature oblique tip intensity profile with fiber in the 0° orientation.

In order to create a chart with a response relative that of the 90° orientation intensity, the integration time was kept constant (1200 ms) and the average maximum intensity observed during the previous four runs at the 90° orientation was used to normalize the 0° orientation response.

5.1.2.4 180° orientation; experimental results

The following chart (Figure 5.8) shows the response obtained from the experiment performed with the fiber in the 180° orientation relative to the optical axis. The iris was set to 3mm.

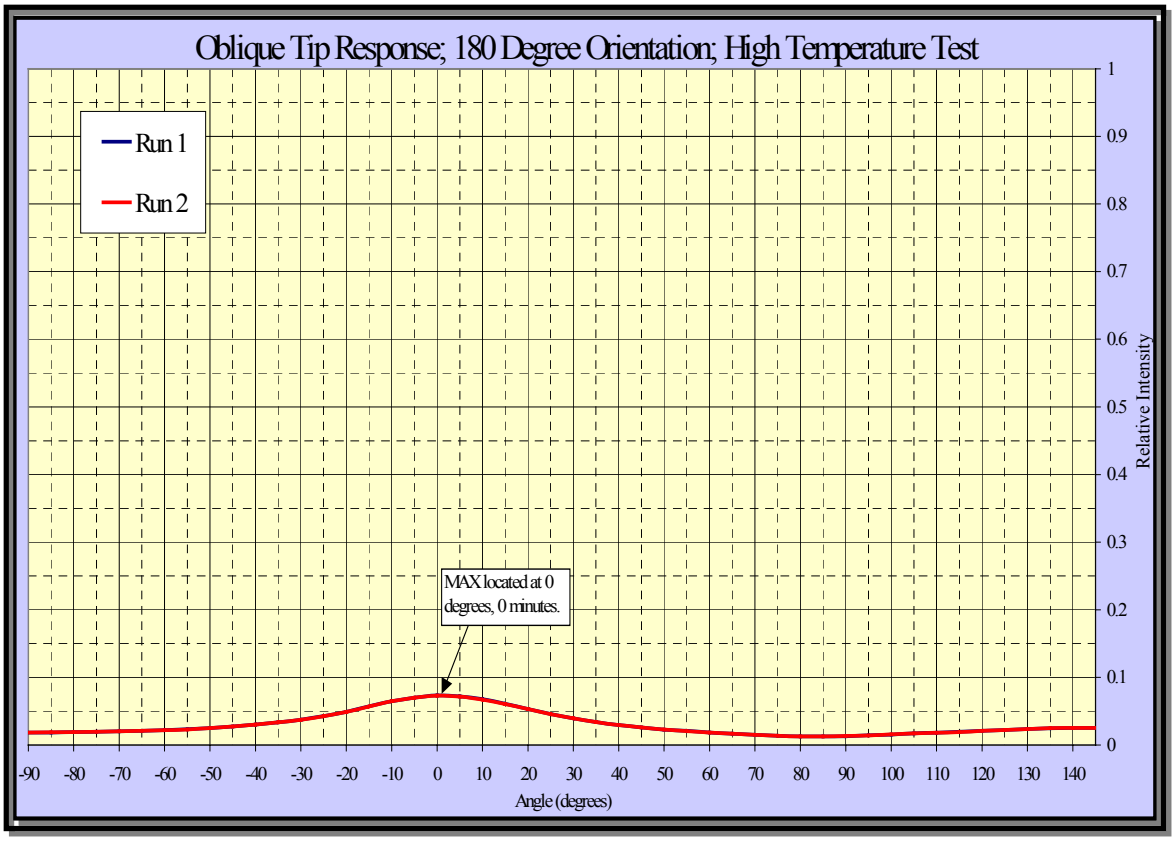

Figure 5.8: High temperature oblique tip intensity profile with fiber in the 180° orientation.

As with the 0° orientation, the response was normalized relative to the average of the maximums observed in the 90° orientation.

5.2 Low temperature measurements

For all practical purposes, the response from incident low temperature radiation was expected to be similar to that observed with the high temperature measurements. Nevertheless, since the index of refraction of sapphire has a slight variation within the range of temperatures examined, it was necessary to reproduce the general response at longer wavelengths. As previously mentioned, the variable aperture diameter experiment was executed to measure the flat tip fiber acceptance angle. The angular scan method was used to measure the angular response of the oblique tip fiber.

5.2.1 Flat tip fiber

Use of the blackbody cavity posed problems in determining the acceptance angle of the flat tip fiber when applying the angular scan method. It was therefore necessary to employ the method presented by Photran. This presented an opportunity to truly test the numerical aperture presented by the manufacturer.

The lead sulfide (PbS) sensor was used to measure the level of intensity incident upon the fiber tip as the iris diameter was increased incrementally. The output peak-to-peak voltage was monitored using the LabVIEW virtual instrument oscilloscope and recorded for each 0.5 mm increase in aperture diameter. In contrast with the intensity measurements made at high temperature, the voltage response was not normalized. Each voltage intensity value was then plotted on a semi-log scale as a function of aperture diameter. This allowed for the response to be monitored such that the leveling off of the curve signified the point at which no additional radiation was being received by the optical fiber.

To ensure that the observed leveling off response was not simply a result of PbS sensor saturation, a neutral density filter was placed between the radiation source and the aperture. The experiment was then repeated under the same guidelines.

5.2.1.1 Test #1; experimental results

The following chart (Figure 5.9) displays the response obtained from Test #1 without and with the filter present.

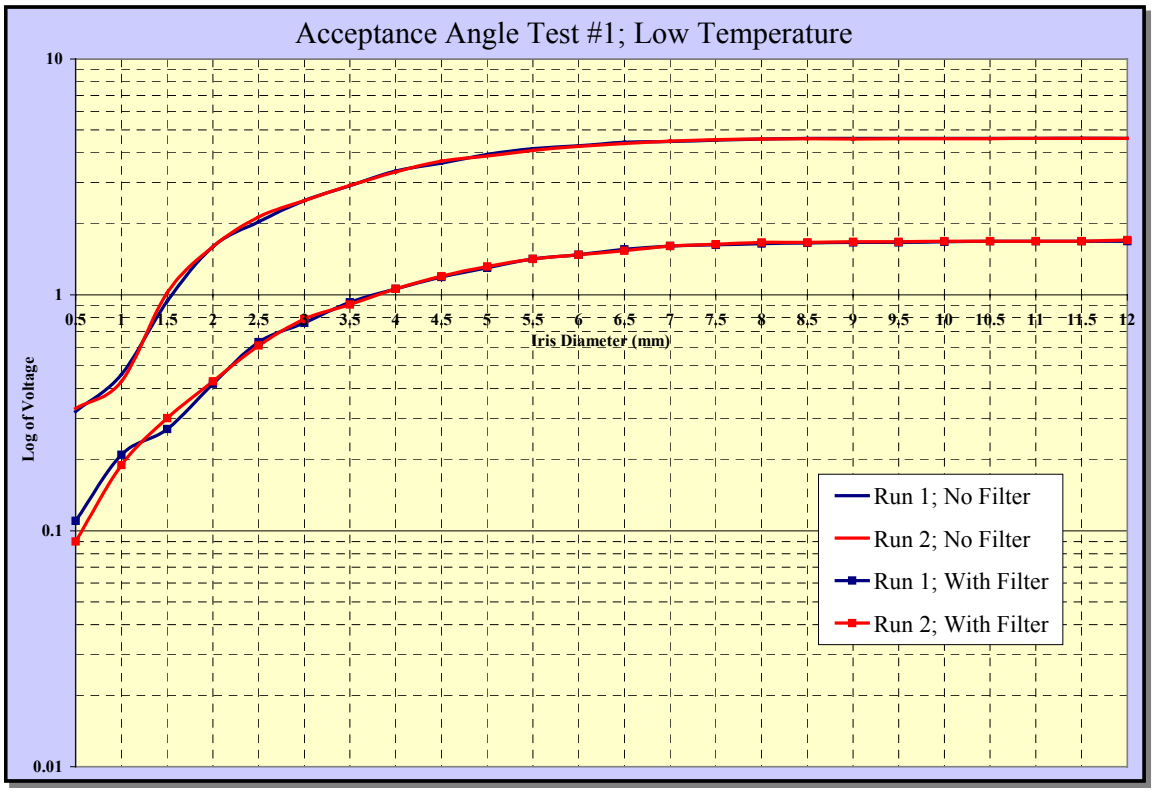

Figure 5.9: Low temperature flat tip acceptance angle results using variable aperture diameter technique; Test #1.

5.2.1.2 Test #2; experimental results

The following chart (Figure 5.10) displays the response obtained from Test #2 without and with the filter present.

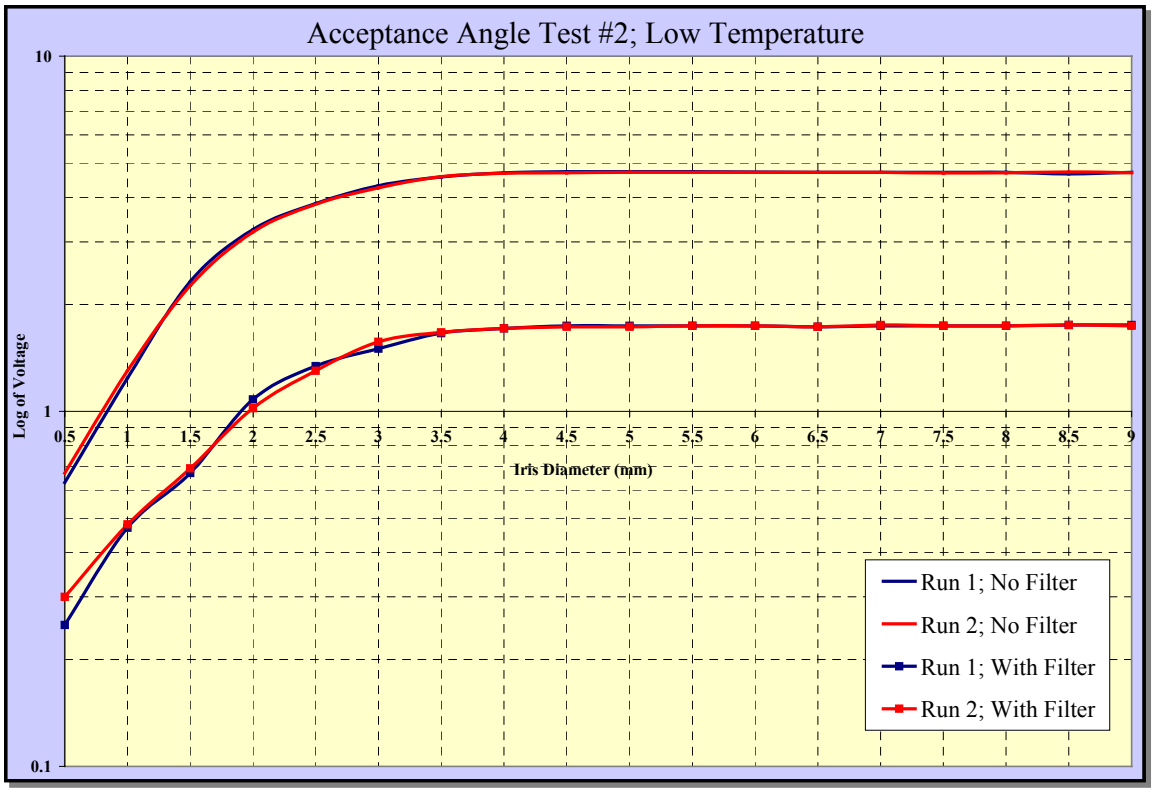

Figure 5.10: Low temperature flat tip acceptance angle results using variable aperture diameter technique; Test #2.

5.2.2 Oblique tip fiber

The angular scan method was employed to measure the oblique tip intensity profile at low temperature. As a consequence of the blackbody cavity size and the constraints of the fiber mounting system, the scan region was reduced to encompass the known area of intensity response. A region spanning -25° to +100° was used for the 90° orientation tests and -25° to +25° was used for the 0° orientation tests. The central axis of the optical fiber is estimated to coincide with the location of maximum voltage intensity observed in the 0° orientation tests. Since the 0° and the 180° orientation experiments performed at high temperature revealed similar responses, the 180° orientation was eliminated from examination at low temperature. The 3 mm aperture plate attachment was used for all test performed.

A similar impeded intensity response was experienced in the low temperature tests. Therefore, the sensor gain amplification was activated to register a suitable voltage response. Voltage intensity measurements were taken at increments of 5°. The resulting response was normalized by the peak value observed and plotted as a function of rotation angle. In contrast to the high temperature tests, no refined increment measurements were taken to isolate the hump, valley, or peak.

The noticeable difference in intensity profile obtained in theses experiments versus the high temperature measurements is the variance among runs taken per test procedure. At high temperature, the intensity profiles are virtually identical (see Figures 5.5-5.8 where the runs are indistinguishable). As for the low temperature tests, the graphs show greater experimental uncertainties at lower relative intensities. This is due

to the difficulty in aligning the fiber accurately with the 3 mm aperture on the blackbody cavity.

5.2.2.1 90° orientation; Test #1; experimental results

The following chart (Figure 5.11) shows the response obtained from Test #1 with the fiber in the 90° orientation relative to the optical axis. The fixed aperture of 3 mm diameter was used. The angular scan ranged from -25° to +100° showing the important characteristics of the intensity profile.

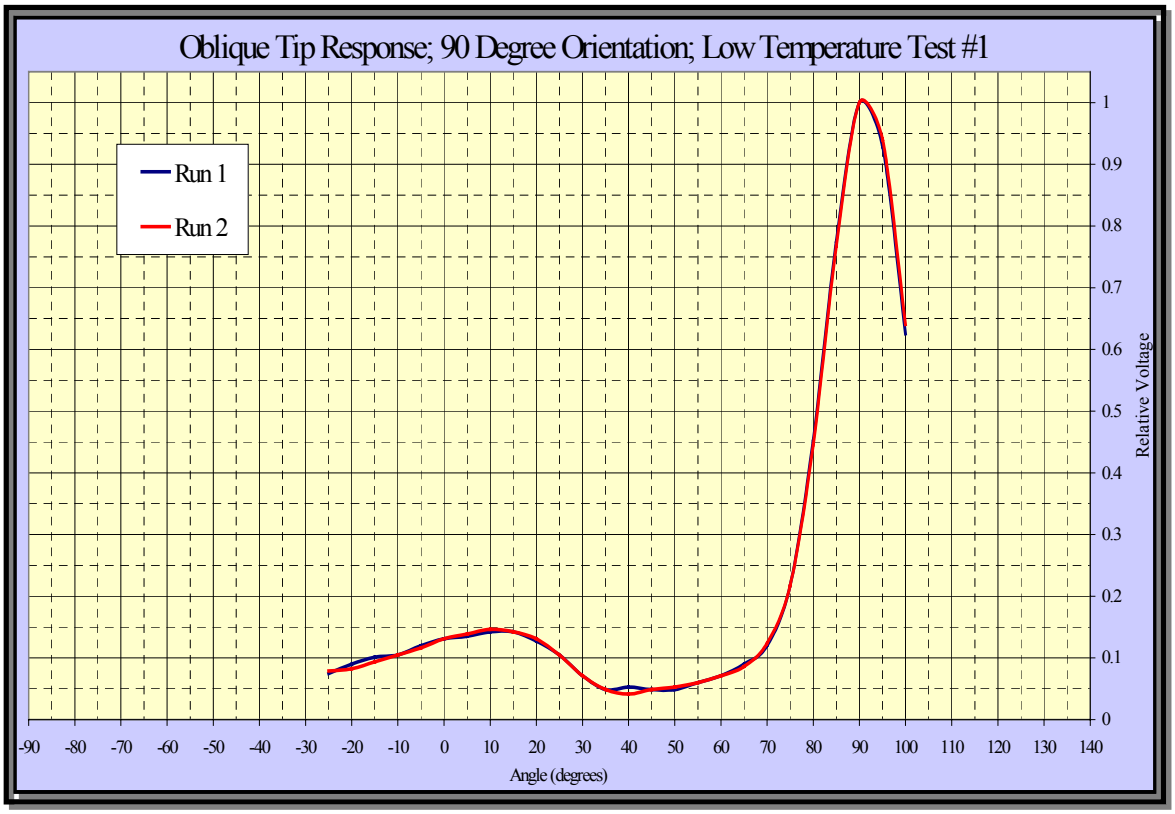

Figure 5.11: Low temperature oblique tip intensity profile with fiber in the 90° orientation; Test #1.

5.2.2.2 90° orientation; Test #2; experimental results

The following chart (Figure 5.12) shows the response obtained from Test #1 with the fiber in the 90° orientation relative to the optical axis. The fixed aperture of 3 mm diameter was used.

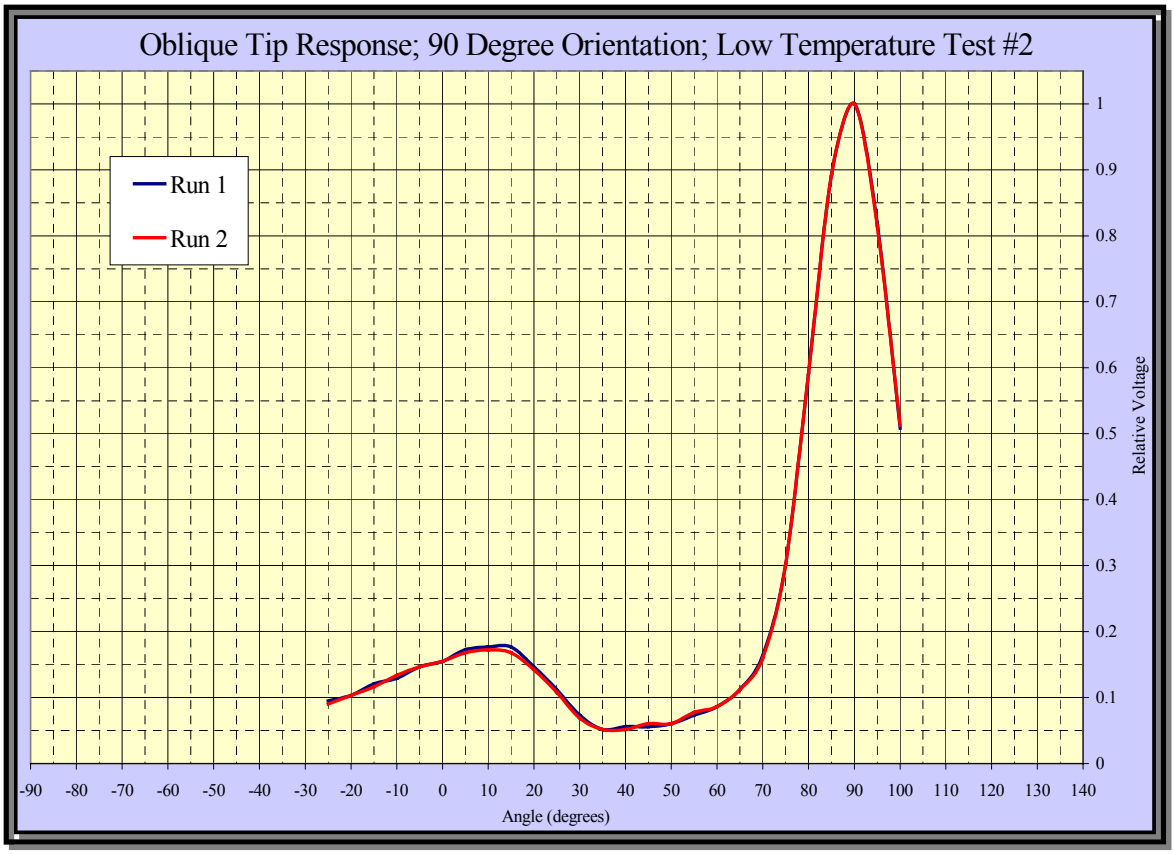

Figure 5.12: Low temperature oblique tip intensity profile with fiber in the 90° orientation; Test #2.

5.2.2.3 0° orientation; Test #1; experimental results

The following chart (Figure 5.13) shows the response obtained from Test #1 with the fiber in the 0° orientation relative to the optical axis. The fixed aperture of 3 mm diameter was used. The angular scan ranged from -25° to +25° showing the important characteristics of the intensity profile.

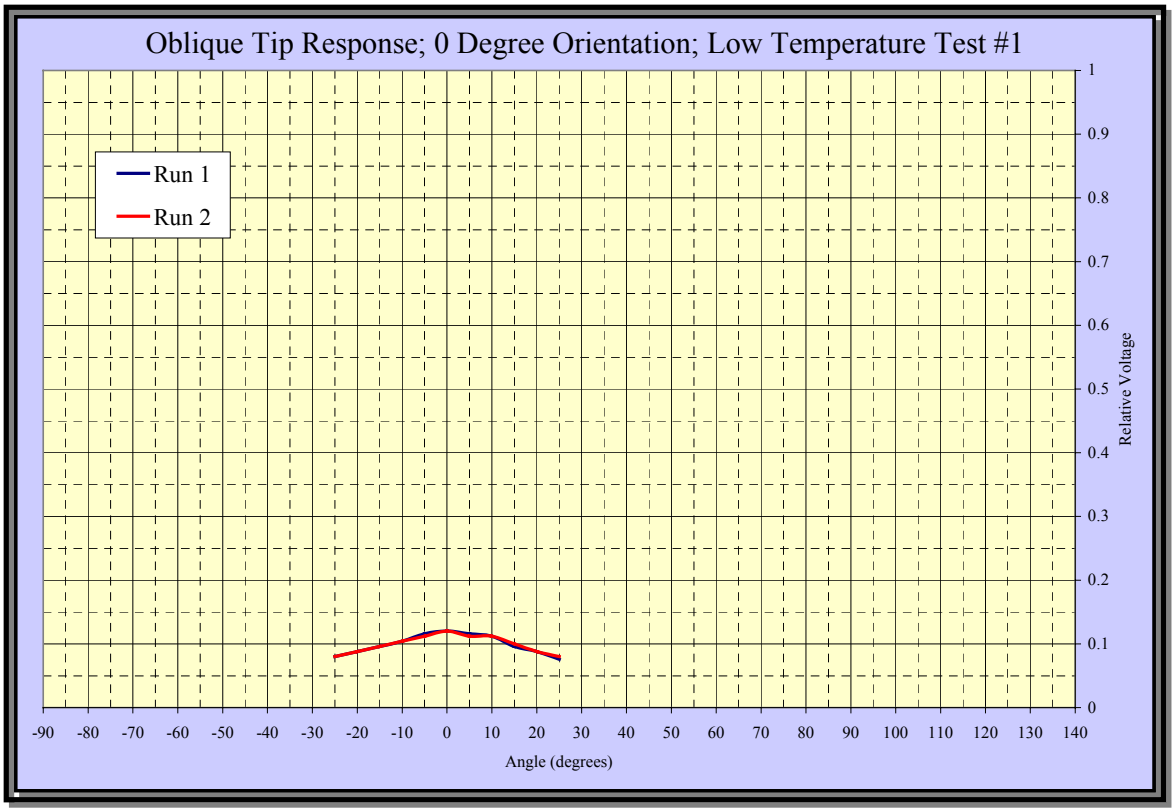

Figure 5.13: Low temperature oblique tip intensity profile with fiber in the 0° orientation; Test #1.

5.2.2.4 0° orientation; Test #2; experimental results

The following chart (Figure 5.14) shows the response obtained from Test #1 with the fiber in the 0° orientation relative to the optical axis. The fixed aperture of 3 mm diameter was used.

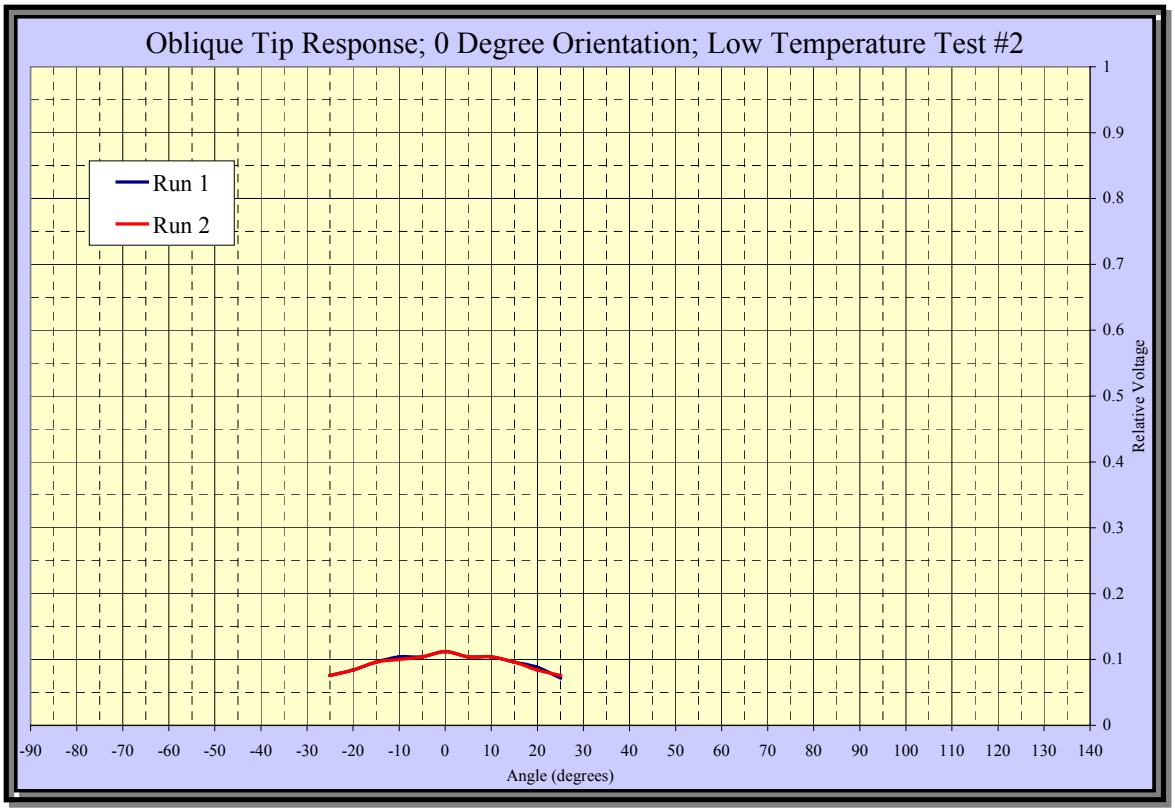

Figure 5.14: Low temperature oblique tip intensity profile with fiber in the 0° orientation; Test #2.

6 Discussion of Results

The following sections provide a detailed interpretation of the results obtained during the entire experimental process. Of particular concern is the response observed by the oblique tip fiber since its future application in temperature measurement is the focus of this research. Accordingly, extensive attention will be paid to the response of the oblique tip optical fiber.

6.1 High temperature measurements

6.1.1 Flat tip fiber

As previously stated, the high temperature tests performed to measure the acceptance angle of the flat tip optical fiber encompassed an angular scan of 30° to ensure the entire intensity profile was captured. Since the intensity distribution obtained in Test #1 and Test #2 resulted in identical conclusions, the two are discussed simultaneously. Additionally, it should be noted that the main purpose for determining the acceptance angle of the flat tip fiber was to validate the experimental configuration.

6.1.1.1 Tests #1 and #2

In total, 8 runs were conducted over the two tests. Half the runs were conducted with the aperture diameter set to 1 mm while the remainder had the aperture diameter increased to 3 mm. In all experiments, the expected symmetric intensity distribution was observed. The acceptance angle, as defined by the IEC standard five percent intensity angle, was observed to be 9°, ±0.5°, for all runs performed.

The quoted acceptance angle provided by Photran, 6° to 7° half-angle for 85% of nominal transmission, required the numerical integration comparison. After analyzing the curve fit data for each experiment performed, the intensity present within the acceptance cone defined by integrating over the limits of ±6° ranged from 85.8% to 87.8%. These results are congruent with the specifications provided by the manufacturer. The relatively small variance obtained from these experiments certifies the results and ultimately validates the experimental configuration as an appropriate means of quantifying the acceptance angle. Furthermore, the numerical integration method can thereby be considered a suitable means of comparing the angular scan method to the variable aperture diameter method.

6.1.2 Oblique tip fiber

6.1.2.1 90° orientation

Two tests were performed to quantify the response of the oblique tip optical fiber at an orientation of 90° relative to the optical axis. In both circumstances, a similar intensity distribution was observed.

With the tungsten halogen light source pointing toward the cut face of the optical fiber, the response was virtually non-existent. The level of response present, roughly 2.5% of the peak intensity, is a result of the large integration time (IT) associated with taking these measurements. Since the IT can be equated to the amount of time an aperture is open on a camera while a picture is taken, greater levels of ambient light will be accepted by the spectrometer as the IT increases. It is therefore appropriate to consider the level of intensity at this angle to be effectively zero though stated relative values do not reflect this adjustment.

The effective zero response remains present from the -90° angle through the -40° angle. At this point the intensity begins to gradually increase. Over the next 30°, the gradual increase in intensity reaches a relative value of 5%. Of interest is the value of relative intensity at the 0° position; approximately 7.5%. At this angle the light source is pointing directly along the optical axis of the fiber yet the graph shows that intensity continues to have an upward slope. This is the first indication of an asymmetric response theoretically predicted by previous research [10,11]. Furthermore, the idea of having a well-defined acceptance angle has, for all practical purposes, been eliminated. That is, a sapphire fiber with a flat tip face only displays an intensity response from ±9° under the angular scan method performed in this research. Conversely, the oblique tip fiber is now responding to incident radiation at an angle 4 times as large.

The intensity response continues to increase at a consistent level until the light source reaches approximately +18° beyond the optical axis. At this point, the slope goes to zero corresponding to a relative intensity approaching 12%. This point is termed the hump. As the angular scan continues, the intensity level begins to decreases at a rate twice a steep as the earlier observed upward slope. This decrease is halted as the rotation angle approaches +47° and the relative intensity response levels off at the previously discussed 2.5% value. Again, the response has effectively reached zero.

This would correspond to an acceptance cone extending from -40° to around +45°. This cone size is significantly larger than that of the flat tip fiber with the principal difference being the vast increase in integration time needed for the oblique tip fiber to register a noticeable response. Initially, this asymmetric response was believed to be the extent of the light gathering capability of the oblique tip optical fiber. However, based on

the low relative values presented thus far, it is obvious that the response continued to increase as the angular scan progressed.

Almost as soon as the response approached a minimum, termed the valley, it began to increase. After the valley, as the angular scan increased to +70°, the rate of relative intensity increase was consistent with the negative of the slope experienced following the hump. This changed dramatically as the scan progressed toward the +90° angle.

From +70° to +90°, the relative intensity response peaks to a value 10 times the level present at the hump. At this angle, the light source is pointing directly toward the cylindrical side of the fiber tip, opposite the cut face. Incremental increases in the angular scan show the increase ceases at an angle of approximately +94°. Appropriately, this location is termed the peak.

Continuing with the angular scan results in an intensity drop at a rate equal to that experienced while approaching the peak. The symmetric peak response generally covers a width of approximately 50°; from +70° to +120°. As the rotary table continues to the +145° angle, the response has descended to below the 5% relative intensity level. Due to physical limitations in the construction of the experimental setup, no readings could be performed beyond +145°. It is therefore assumed that the response continues toward the effective zero point, 2.5%, as previously defined.

Why this response occurs is inevitably the next question. The unmistakable answer is due to a prism effect caused by the radiation reflecting off the inside cut surface of the optical fiber tip. This belief was ultimately verified by previous research discovered subsequent to these experimental results. Essentially, all light entering the

optical fiber from the side opposite the cut face refracts at the surface interface then reflects off the internal side of the cut tip. The angle of incidence is greater than the critical angle necessary to cause total internal reflection causing the photons to be coupled down the fiber. When the light source is in the general area of the 90° position, the sensor receives the greatest amount of totally internally reflected radiation and the intensity response achieves a maximum. Through the use of ray tracing techniques, a more comprehensive explanation of this occurrence is provided in the theoretical/empirical section of this thesis. The full intensity distribution, from -90° to +145°, is examined.

An attempt was made to obtain a visual understanding of this observed response. By coupling the light source directly to the sapphire optical fiber, the light emitted from the tip could be seen. The initial intention was to measure the spot size emitted from the fiber surface, however, the minute output intensity was difficult to photograph. The illumination present on the surface of the fiber was therefore photographed. Figure 6.1 a) shows the output from the sapphire optical fiber analogous to the light source pointing in the +90° position on the rotary table. That is, the light emitted at this surface provides an idea of the acceptance capabilities in a similar orientation. By rotating the fiber about the optical axis 180°, Figure 6.1 b) shows the light output analogous to the light source being placed in the -90° position; the starting position in this experiment. It is therefore obvious, from a qualitative standpoint, why the

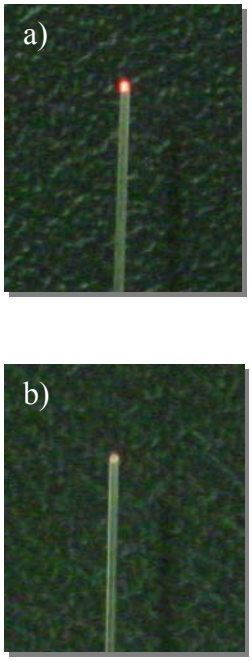

Figure 6.1: Radiation emitted from the fiber tip when cut face is, a) pointing downward and, b) pointing upward.

resultant intensity response pattern has its shape. As an aside, notice the color of the transmitted light emitted from the sapphire fiber. The light source emits white light, however, the fiber output is red. The red color is consistent with the predominant transmission of longer wavelengths in the visual spectrum due primarily to Rayleigh scattering.

It is important to note that the 270° fiber orientation was not examined. From cursory measurements taken during the experimental process, it was concluded that the response was identical to that experienced by the 90° fiber orientation with the sign of the angle values reversed. That is, the response at -90° is present at +90° and the response at +145° is present at -145°.

6.1.2.2 0° and 180° orientation

As seen in Figures 5.7 and 5.8, the data received from the experiments performed with the fiber oriented at 0° and 180° resulted in identical intensity profiles. As previously stated, the data was normalized by the average of the four maximum intensities observed during the 90° orientation experiments. For all runs, the light source was originally placed at the -90° position on the rotary table and rotated at 5° increments to +145°.

As is observed from the plotted values of relative intensity, the large integration time allowed for excessive ambient light to be accepted by the spectrometer. This is again present in a nominal response at the 2.5% level. As before, this can be considered an effective zero intensity level.

In direct comparison to the results obtained in the 90° orientation experiments, the fiber begins to respond at the -70° angle versus the -40° angle. The slope very gradually

increases over the next 70° leveling off at the 0° angle position. The relative intensity has a maximum value of roughly 7.5%. This is less than the value observed at the hump location in the 90° orientation experiment. As angular rotation continues, the response decreases at an equivalent rate toward the +70° rotation angle.

The symmetric intensity distribution was expected with respect to these particular orientations. However, the light gathering ability was thought to be greater than that seen experimentally. It appears that the incident radiation is predominantly reflecting off the cut face with minimal transmission occurring as the radiation source approaches the 0° angle of rotation. Since the relative intensity is significantly lower than that obtained at the 90° orientation, it is deemed inconsequential to explore a theoretical explanation with ray tracing techniques.

6.2 Low temperature measurements

The purpose of these experiments was to obtain a similar intensity profile as that observed at high temperature. Having been enlightened previously to the intensity distribution of the oblique tip fiber, verification of a similar low temperature response was necessary since the refractive index of sapphire has modest wavelength dependence within the temperature range examined. The low temperature measurements do not possess the same level of accuracy present in the high temperature data. This is due in large part to the difficulty in precisely aligning the experiment due to the large size and off centered output of the blackbody cavity.

6.2.1 Flat tip fiber

Isolating an aperture for low temperature measurements of the flat tip fiber acceptance angle proved to be difficult when using the blackbody cavity radiation source since the entire face emitted radiation. The variable aperture diameter experiment was therefore conducted. This experiment was more inline with the manner in which Photran specified the numerical aperture.

6.2.1.1 Test #1

Recall that in this experiment, the acceptance angle is derived by monitoring the change in intensity received by the sensor as the aperture diameter increases. As can been seen from the graphical response curve obtained from Test #1, the plateau begins when the aperture diameter reaches between 7 and 7.5 mm. The trigonometric relationship between the aperture diameter and the placement of the fiber behind the aperture, 30 mm in this experiment, results in an acceptance angle of 6.6°. This result remains consistent when evaluating the graphical data obtained with the neutral density filter included. The value of acceptance angle corresponds to a numerical aperture of 0.115, which is within the range provided by the manufacturer.

6.2.1.2 Test #2

The difference between Test #1 and Test #2 is that the location of the fiber behind the aperture was decreased from 30 to 20 mm. Apparent from the graphical representation of voltage intensity, the plateau begins between an aperture diameter of 4 to 4.5 mm. A consistent response is obtained with the neutral density filter present. According to the trigonometric relationship, the acceptance angle is therefore roughly

6.4° with a corresponding numerical aperture of 0.111. Again, this value is within the range provided by the manufacturer.

6.2.2 Oblique tip fiber

When measuring the oblique tip intensity response, the problems observed during the flat tip experiments were not present. There was however, difficulty present in accurate fiber, radiation source, and rotary table alignment. The alignment was not as precise as that achieved in the high temperature experiments. Nevertheless, aspirations of achieving a generally similar response negated the concern associated with a lack of high precision.

6.2.2.1 90° orientation

Figures 5.11 and 5.12 show the intensity profile obtained from the two tests conducted in validating the response of the oblique tip fiber in the 90° orientation. The results of both experiments are similar and therefore discussed as one. Due to the large size of the low temperature radiation source, the scan was limited to a region spanning from -25° to +100°. Regardless, the intensity distribution does show a general resemblance to the distribution obtained at high temperature.

Beginning at the -25° angle the response is increasing at a steady rate through the point representing the optical axis of the fiber, the 0° rotation angle. The signature hump occurs between +10° and +15° at a relative voltage intensity around 15% to 17%. This relative intensity is greater than that observed during the high temperature measurements and can be directly attributed to the fiber not being positioned in the exact 90° orientation with respect to the optical axis.

As before, the asymmetric response descends at a rate similar to that experienced at high temperature; roughly twice the rising rate. The valley occurs near the +40° angle, shortly before the previous valley observed at high temperature. The relative intensity then begins to increase almost immediately, first slowly to the +70° angle then rapidly to the peak at +90°. The peak is followed by a swift decline in slope toward the zero position. Since the table rotation was limited to the +100° angle, it is assumed that further response is identical to that observed at high temperature based on the previous similarities witnessed.

The results obtained from these experiments provide validation to the previous statement regarding the sapphire optical fiber having an identical intensity profile at low temperature as that at high temperature.

6.2.2.2 0° orientation

Since the response at the 0° and 180° orientation was discovered to be identical at high temperature, low temperature measurements were made only for the 0° orientation. As with the above 90° orientation, the two test conducted at 0° orientation produced results so similar that the collection is discussed together.

The range of angular scan was limited to the region encompassing -25° to +25°. Based on the similarities thus far experienced, inspection outside this region was deemed unnecessary. Ultimately, the intensity distribution was identical to that observed at high temperature. A maximum value was observed at the 0° angle of rotation with a relative voltage of around 12%. As seen at high temperature, this value is less that the hump value received in the 90° orientation. The expected symmetric response therefore proved to be present in this orientation.

6.3 Intensity difference

Second to the intensity profile of the oblique tip optical fiber at the 90° orientation, the difference in radiation gathering capability between the flat tip and oblique tip fibers poses an interesting issue. During high temperature measurements, why is it necessary to increase the integration time by a factor of 45 such that the oblique tip fiber can accept the same number of photon as the flat tip fiber? Additionally, for low temperature measurements, the sensor gain amplification had to be used to register a response.

As can be seen from the photographs in Figure 6.2, the intensity output from the flat tip sapphire optical fiber is markedly greater than that observed from the oblique tip fiber in any orientation. Regarding the oblique tip fiber, the output intensity present from the orientation associated with the peak response pails in comparison to the flat tip fiber; comparing a) to c).

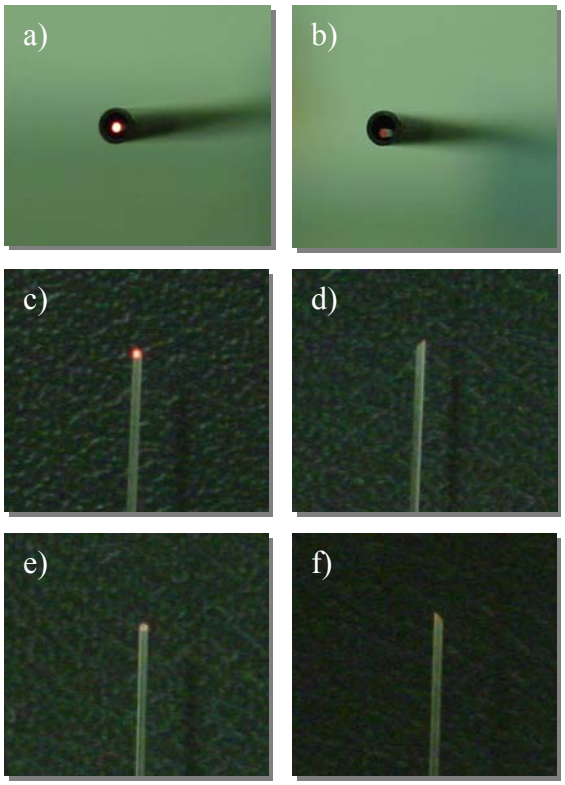

Figure 6.2: Visualization of radiation intensity emitted from, a) the flat tip optical fiber (head on), b) the oblique tip fiber (head on), c)-f) various angles around the oblique tip fiber.

By now it is indisputable that the oblique tip fiber accepts the greatest amount of radiation along the curved surface opposite the cut tip. This surface geometry is believed to contribute to the reduction in photon acceptance and subsequent increase in integration time of the

spectrometer. It is therefore postulated that the acceptance of incident radiation by the oblique tip fiber is hindered by the curved surface geometry when compared directly to the flat tip fiber.

It stands to reason that a considerable amount of radiation normally incident on the cut surface will reflect off at an angles hindering photon transmission and resulting in the response observed in the 0° and 180° orientations relative to the optical axis. A similar occurrence is theorized for the 90° orientation as a consequence of cylindrical surface geometry. This is examined in greater detail in the theoretical/empirical section of this thesis.

7 Theoretical/Empirical Evaluation

Purely theoretical models do not provide an adequate explanation of the results obtained from these experiments. Therefore, the inclusion of adjustments to the theoretical models is made to coincide with the empirical data. The following sections attempts to rationalize the observed intensity distribution.

7.1 Flat tip fiber

Though wavelength dependence exists, the refractive index of sapphire is approximately 1.75 within the temperature range of the experiments conducted for this research. The index of refraction of air is 1.00. Through the use of Snell's Law, a theoretical derivation of the critical angle θ_c and the acceptance angle θ_{max} of an unclad, flat tip sapphire optical fiber can be formulated and computed [24].

$$n_i \sin\theta_i = n_t \sin\theta_t \tag{7.1}$$

$$\theta_c = \sin^{-1}\left(\frac{n_t}{n_i}\right) = \sin^{-1}\left(\frac{n_a}{n_s}\right) \tag{7.2}$$

$$\theta_{\max} = \sin^{-1}\left(\frac{\left(n_t{}^2 - 1.0\right)^{\frac{1}{2}}}{n_i}\right) = \sin^{-1}\left(\frac{\left(n_s{}^2 - 1.0\right)^{\frac{1}{2}}}{n_a}\right) \tag{7.3}$$

where :

n_i is the index of refraction of the incident material
θ_i is angle of incidence
n_t is the index of refraction of the transmitted material
θ_t is the angle of transmission
n_a is the index of refraction of air
n_s is the index of refraction of sapphire

The reversal of n_a and n_s in the equations for θ_c and θ_{max} reflects the change in traversing material. The critical angle θ_c is calculated to be 34.9°. Based on the theoretically undefined value of acceptance angle θ_{max} (corresponding to the maximum 90° half-angle), all light incident on the fiber face should be coupled down the fiber. Yet, from the experiments conducted in this research, it is evident that this value is grossly overstated. Even accounting for reflection according to the Fresnel equations, the acceptance angle of 9° obtained from the angular scan method cannot be theoretically deduced.

The conflict between theoretical and empirical values of numerical aperture is considered conventional simply by inserting the term "effective." Aptly, the effective numerical aperture of the sapphire optical fiber is 0.10 to 0.12 as dictated by the manufacturer. Under a similar logic, it can be stated that the sapphire optical fiber possesses an effective acceptance angle θ_{max_eff} of 9° as determined by the angular scan method. Through the use of ray tracing techniques, this translates to an effective critical angle θ_{c_eff} within the fiber of 84.9°. It can therefore be postulated that for internal incident angles smaller than θ_{c_eff}, a fraction of the radiation will be reflected down the fiber while the remainder is transmitted out through the fiber wall. This reasoning is precisely aligned with the existing theoretical model of incident rays interacting with the fiber wall at angles less than the critical angle.

The effective critical angle θ_{c_eff} provides a means of quantifying the maximum number of wall reflections present along the length of the fiber propagating without leakage. Since the optical fiber diameter is 0.425 mm, a reflection occurs every 4.76 mm. Along the 1 m length of the optical fiber tested, this translates to roughly 210 reflections

assuming a perfectly straight fiber. Therefore, wall reflections greater than 210 will cause rays to leak out quickly, reducing or eliminating the response received by the optical sensor.

Along the length of the fiber, the presence of impurities within the fiber leads to radiation attenuation due to Rayleigh scattering. The shorter the distance necessary for a ray to travel, the less scattering occurs. Conversely, the greater the distance traveled, the greater the scattering. The effects of Rayleigh scattering account for, 1) the reddish color observed at the terminal end of the fiber since longer wavelengths are less effected by scattering and, 2) the maximum intensity distribution along the axial mode.

7.2 Oblique tip fiber

Ray tracing techniques, along with the previous discussion on the effective critical angle θ_{c_eff} and maximum number of internal reflections, largely explain the response observed for the oblique tip optical fiber. Beginning at the -90° position, a single ray path was followed as it interacted with the face and internal walls of the oblique tip fiber in the 90° orientation. That is, the first ray strikes the cut face at an angle of -45° to the surface normal. This process continued at increments of 15° toward the +135° position such that the incident wall angles could be determined as a function of angular rotation. The individual ray tracings are attached in Appendix A.

The observed angular response of the oblique tip fiber is a combination of the following factors:

1) Reflection and transmission along the external surfaces.

    a) The planar cut face.

b) The cylindrical surface opposite the cut tip face.

2) The internal angle of incidence at the wall reflections.

3) The number of wall reflections within the fiber.

4) Reflection and transmission along the internal surfaces.

a) The planar cut face.

b) The cylindrical wall along the length of the fiber.

Due to the complexity associated with the fiber surface curvature, a single plane along the central axis and through the full length of the cut face was evaluated to simplify the ray tracing procedure. This simplification is deemed appropriate since this plane coincides with the 90° fiber orientation examined in this research.

Table 7.1 lists theoretical values of the afore mentioned factors resulting in the responses obtained from the experiments:

Table 7.1: Tabulated angles and percentages of reflection and transmission to various angles of incident radiation. Also, the number of internal reflections experienced by a transmitted ray.

Angular Position of Radiation Source	External Incident Angle	Total External Reflectance	Total External Transmittance	Internal Incident Angle	Number of Internal Reflections
-90°	-45°	8.6%	91.4%	21.2°	2194.2
-75°	-30°	7.6%	92.4%	28.4°	2069.8
-60°	-15°	7.4%	92.6%	36.5°	1891.6
-45°	0°	7.4%	92.6%	45.0°	1663.8
-30°	15°	7.4%	92.6%	53.5°	1399.4
-15°	30°	7.6%	92.4%	61.6°	1119.1
0°	45°	8.6%	91.4%	68.8°	849.6
15°	60°	12.8%	87.2%	74.7°	622.4
30°	75°	28.8%	71.2%	78.5°	469.0
45°	90°	100.0%	0.0%	79.8°	414.7
60°	30°	7.6%	92.4%	73.4°	672.3
75°	15°	7.4%	92.6%	81.5°	348.0
90°	0°	7.4%	92.6%	90.0°	0.0
105°	-15°	7.4%	92.6%	81.5°	348.0
120°	-30°	7.6%	92.4%	73.4°	672.3
135°	-45°	8.6%	91.4%	66.2°	950.7

By comparing the internal incident angle and the number of internal reflections to the values of effective critical angle θ_{c_eff}, 84.9°, and the maximum wall reflections, 210, computed during the discussion on the flat tip fiber, the total internal reflectance and transmittance can be inferred and are therefore excluded from this data table. The highlighted rows indicate the position of the hump, valley, and peak. Each location will be discussed individually.

7.2.1 Hump

The response observed during the experiments at angles of rotation between -90° and -40° was non-existent. Since the value of internal reflection is consistently dropping prior to the -40° position, it can be supposed that the fiber leaks all radiation when there are roughly 1600 or more internal reflections corresponding to an internal incident angle of approximately 47°. As was observed during the experiments, the intensity begins to slowly increase at the -40° position. This increase is again attributed to the decrease in the number of internal reflections as modest amounts of radiation are transported along the length of the fiber.

The hump was observed experimentally to exist around the 18° position of rotation. At 15° in the theoretical model, the number of internal reflections, 622.4, indicates that a significant portion of the incident radiation continues to be lost through the wall of the fiber. With a lower number of internal reflections at 30°, 469.0, increased intensity received by the sensor would be expected. This can also be concluded by the larger internal incident angle; 78.5° versus 74.7° at 30° and 15° respectively. Experimentally however, this is not the result. It is therefore believed that the value of total external transmittance, 87.2% relative to 71.2%, is the dominant factor for the

maximum intensity observed at the hump. That is, by allowing more radiation to enter the fiber, the other aspects contributing to sensor response become less important.

Furthermore, it is thought not to be merely coincidence that the hump is located at the angle of rotation defining the Brewster angle. The Brewster angle is a function of the refractive indices of the fiber material and the submersing medium; sapphire and air respectively. It is mathematically defined as follows [24]:

$$\theta_p = \tan^{-1}\left(\frac{n_t}{n_i}\right) = \tan^{-1}\left(\frac{n_s}{n_a}\right) \tag{7.4}$$

where θ_p is the Brewster angle

At this angle, only the perpendicular component of the incident radiation is reflected along the air/sapphire interface as shown in Figure 7.1. This indicates that the strength of the transmitted radiation increases thereby increasing the sensor response. With a refractive index of 1.75 and 1.00 for sapphire and air respectively, the Brewster angle is 60.3°. With respect to the surface normal of the cut face, this position is just slightly beyond the 15° angle of rotation. The amount of reflection occurring on the surface grows quickly

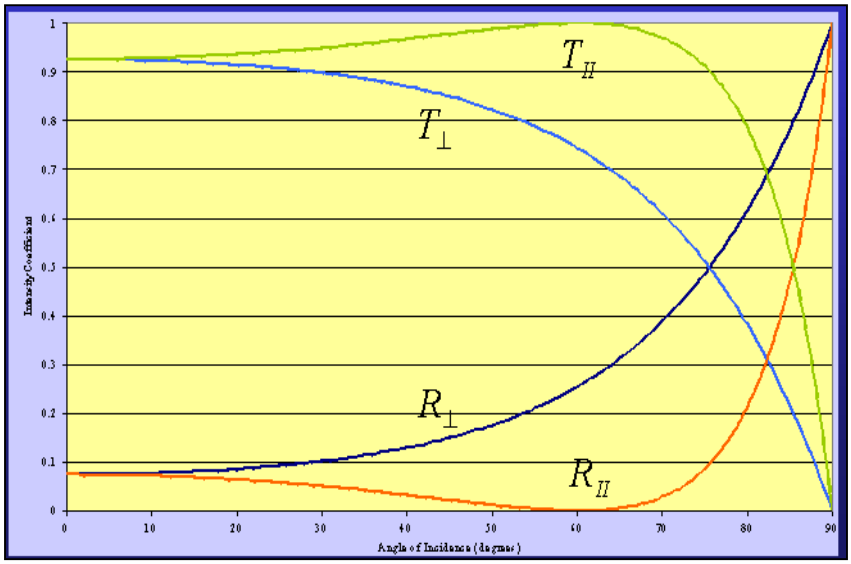

Figure 7.1: Perpendicular and parallel components of transmittance and reflectance for air/sapphire interface.

as the angle of rotation is increased leading toward the valley thereby lowering the intensity response.

7.2.2 Valley

The location of the valley can be determined theoretically simply through the use of the Fresnel equations. The rotation angle of +45° corresponds to an incident angle of 90° with respect to the surface normal along the cut face. With the incident ray pointing directly along the surface of the cut face, it is shown that 100% will reflect off the surface with 0% refraction. However, the data table indicates the presence of internal reflections at this position of angular rotation. This result is directly related to the inability of Snell's Law to account for external surface reflections.

It can be argued theoretically that this position is also the 45° position pointing at an angle along the cylindrical surface of the fiber opposite the cut face. Under this model, the number of internal reflections and internal incident angle would be 950.7 and 66.2° respectively. This, too, would result in a nominal response from the sensor due to the large number of internal reflections. Nevertheless, it is straightforward to explain the observed response as a result of total surface reflection at the 90° incident angle with respect to the cut face.

7.2.3 Peak

All radiation, incident along the cylindrical side of the oblique tip, undergoes refraction at the surface and reflection with the internal side of the planar cut face. The polished planar surface of the cut tip promotes the true response for total internal reflection. That is, incident radiation striking the planar surface at an angle greater than the true critical angle θ_c of 34.85° will totally internally reflect. Along the length of the

cylindrical fiber, the postulated effective critical angle θ_{c_eff} of 84.9° still dominates radiation leakage.

Evident from the ray tracing diagrams in Appendix A, at angles of rotation between +60° and +105°, corresponding to 30° and -15° relative to the surface normal respectively, the incident ray experiences total internal reflection. For the remaining incident angles, -30° and -45° relative to the surface normal, the incident ray transmits a portion of its intensity out of the planar cut face. However, the regions outside ±15° are relatively inconsequential when compared to the area within. This again is due to the high number of internal reflections causing leakage along the length of the fiber.

By isolating the ±15° region, the effects of reduced modes within the fiber can be evaluated. The symmetric results obtained from theoretical calculations are evident in the results observed experimentally. Approaching the peak from either side, the number of internal reflections drops and the intensity reading at the sensor increases dramatically. This is further evident by the increasing incident angle of the ray with the fiber wall. At ±15°, the internal incident angle of 81.5° begins to approach the effective critical angle θ_{c_eff}, 84.9°. Not surprisingly, the internal incident angle equals the effective critical angle at ±9° off the peak. Finally, when the external incident angle coincides with the surface normal along the cylindrical wall, the ray is internally reflected at 90° and sent down the fiber along the axial mode. The corresponding response is at a maximum since there is no interaction with the fiber wall and therefore, no external leakage of radiation.

When comparing the theoretical calculations directly to the experimental observations, a slight discrepancy is evident. The experimental peak is located roughly 4° off the theoretical value of 90°. By shifting the response such that the experimental

peak is precisely aligned with the theoretical peak, the entire response, hump, valley, and peak, concurs with the theoretical assessment with only slight variance. This slight variance further accredits the accuracy and precision inherent to this experimental configuration.

7.3 Intensity difference

As discussed in previous sections, the radiation gathering ability of the oblique tip fiber is considerably weaker than the flat tip fiber. The integration time on the spectrometer had to be increased by a factor of almost 45 in order to obtain the same intensity count. An adequate interpretation of the impeded intensity has not been identified but is believed to be a consequence of the surface geometry of the oblique tip fiber.

The effective surface area of the flat tip and oblique tip optical fiber is 0.142 mm^2 and 0.213 mm^2 respectively. However, the flat tip fiber allows all incident radiation within the acceptance cone to be coupled with nominal surface reflection; 7.4% as computed from the Fresnel equations. Conversely, incident radiation strikes the cylindrical surface at multiple angles. The cylindrical surface of the oblique tip fiber therefore has surface reflection with a greater dependence on the angle of incidence. The only location along the cylindrical surface that closely mimics the surface of the flat tip fiber is the tangent directly opposite the cut face. This coincides with the plane evaluated in ray tracing. At curvature angles off this point, reflection increases allowing less radiation to be coupled into the fiber thereby frustrating the intensity response.

8 Future Research Recommendations

Though this research has presented the reader with a general understanding of the performance capabilities of an oblique tip optical fiber, many questions remain unanswered. Of foremost interest is the response of the angled tip fiber over the full 360° orientation with respect to the optical axis. Due to limitations inherent with the experimental hardware, this research has examined only areas believed to encompass the extremes; orientations at 90° intervals. Precise fiber rotation about the optical axis would provide a means to accurately define the region with which the fiber is capable of accepting incident radiation.

In a similar vein, development of methods aimed at isolating the viewing window should be explored. As presented in this thesis, the 45° tip receives a nominal amount of radiation at an angle off the optical axis. From a relative perspective, this amount is insignificant, however, elimination of this area is preferred. A logical first step would be to test the intensity profile of sapphire fibers with tip angles 60° or greater. This would quickly validate or discount the postulation made regarding a Brewster angle relationship to the hump location. Furthermore, as sapphire growth technology improves, the use of a single mode oblique tip fiber can be explored. This would effectively eliminate the introduction of higher order modes experienced at angles outside the 90° orientation. Theoretically, this isolates the incident radiation to a region directly perpendicular to the optical axis.

The most intriguing question arises from the non-trivial divergence in radiation gathering capability between the flat and oblique tip optical fibers. The cylindrical surface geometry is considered a major factor in hindering the reception of incident

radiation. An option designed to improve this capability would be to polish the cylindrical surface, along the length opposite the cut face, to a planar surface. This would reduce the effects of surface reflection thereby increasing the level of photon transmission.

Finally, the development of an improved theoretical model for quantifying the "effective" response of both flat and oblique tip optical fiber is desired. The present theoretical models, adapted for use in fiber optic theory, simply do not provide an adequate explanation of the true response optical fibers exhibit experimentally.

9 Conclusions

As was stated in the introduction of this thesis, this research is merely a single component in the development of a ceramic filtration device to be incorporated into the exhaust system of Diesel engines. Not to undermine its importance, the efficient removal of particulate matter from within the filter is decidedly dependent on precise thermal mapping achieved through the use of the optical fiber under examination. To that end, this research project has succeeded in presenting the team with a comprehensive means of isolating the region from which the oblique tip sapphire optical fiber will accept incident radiation.

The flat tip optical fiber was determined to have an acceptance angle of 9° when examined using the angular scan technique. Using the variable aperture technique, the numerical aperture, 0.10-0.12, presented by the manufacture was verified for the flat tip fiber. The acceptance angle of the oblique tip optical fiber cannot be defined according to traditional convention. A general acceptance region is therefore defined.

For laser surgical applications, previous research provided an evaluation of the pattern of radiation exiting the oblique tip optical fiber. It was shown that the output pattern was primarily directed at an angle 90° off the central axis of the fiber. The goal of this research program was to accurately characterize the angular response of a 45° angled tip optical fiber accepting radiation. Through the use of the angular scan method, it was confirmed that the majority of incident radiation is received by the fiber in a region perpendicular to the optical axis.

Issues unique to the reception of radiation arose during this research project. Of principal importance is the disparity in radiation gathering ability between the flat and

oblique tip optical fibers. It was surmised that the fiber's cylindrical exterior geometry is the logical cause hindering the acceptance of incident photons due to surface reflections. One solution designed to lessen the impact of this impedance involves polishing the cylindrical surface opposite the cut tip such that a planar acceptance region will resemble that of a flat tip optical fiber.

This research demonstrated that the oblique tip optical fiber is an appropriate tool for measuring wall temperatures within confined spaces not suitable for flat tip geometries. Further research directed at isolating the acceptance region, is suggested to enhance the qualities of the oblique tip sapphire optical fiber.

References

[1] Denisov, Nikolay A. and Igor V. Kravchenko (1996) "Shape-dimension optimization of contact medical laser delivery systems" Biomedical Systems and Technologies SPIE vol. 2928, 46-57.

[2] Mrochen, Michael, Peter Riedel, Christof Donitzky, and Theo Seiler (2001) "Erbium: yttrium-aluminum-garnet laser induced vapor bubbles as a function of the quartz fiber tip geometry" *Journal of Biomedical Optics* vol. 6 no. 3, 344-350.

[3] Rol, Pascal, Urs Utzinger, Dominik Beck, and Peter F. Niederer (1994) "Fiber Beam Shaping and Ophthalmic Applications" *Lasers in Ophthalmology II* SPIE vol. 2330, 56-62.

[4] Russo, Vera, Giancarlo Righini, Stefano Sottini, and Silvana Trigari (1985) "Optical fibres for medical applications: output beam shaping" *Fibre Optics '85* SPIE vol. 522, 166-173.

[5] Russo, Vera, Giancarlo Righini, and Silvana Trigari (1984) "Side Radiation Optical Fibres for Medical Applications" Porphyrins in Tumor Phototherapy, Alessandra Andreoni and Rinaldo Cubeddu eds., Plenum Press, 309-319.

[6] Utzinger, Urs, and Rebecca R. Richards-Kortum (2001) "Fiber Optic Probes for Biomedical Optical Spectroscopy" *Journal of Biomedical Optics*, accepted, 2001, www.u.arizona.edu/~utzinger/

[7] van Vleit, Remco J., David G. Molenaar, Christian FP van Swol, Tom A. Boon, and Rudolf M. Verdaasdonk (1994) " Optical characteristics of side firing fibers for laser prostatectomy" *Biomedical Optoelectronic Devices and Systems II* SPIE vol. 2328, 102-109.

[8] Verdaasdonk, Rudolf M. and Christian FP van Swol (1995) "What makes a fiber tip do the job: an optical and thermal evaluation study" *Biomedical Optoelectronic Instrumentation* SPIE vol. 2396, 37-45.

[9] Verdaasdonk, Rudolf M. and Cornelius Borst (1992) "Modified Fiber Tips: Optical and Thermal Characteristics" *Optical Fibers in Medicine* VII SPIE vol. 1649, 172-183.

[10] Cooney, Thomas F., H. Trey Skinner and S.M. Angel (1996) "Comparative Study of some fiber-Optic Remote Raman Probe Designs. Part I: Model for Liquids and Transparent solids," Applied Spectroscopy, vol. 50, no. 7, 836-848.

[11] Li, Ying-Sing and Jiaying Ma (1997) "Optical-Fiber Raman Probe with Tilted-End Fibers," Applied Spectroscopy vol. 51, no. 2, 277-279.

[12] Ramos, Rogerio T. and Edmond J. Fordham (1999) "Oblique-Tip Fiber-Optic Sensors for Multiphase Fluid Discrimination" *Journal of Lightwave* Technology vol. 17, no. 8, 1392-1400.

[13] Kottmann, Jorg Phillip and Christian Stenzel (1999) "Characterization of Flexible Sapphire Fibers in High-Temperature Pyrometers" *Sensors and Materials* vol. 11, no. 4, 233-246.

[14] Dils, R.R. (1983) "High-temperature optical fiber thermometer" Journal of Applied Physics vol. 54, no. 3, 1198-1201.

[15] Murata, Hiroshi (1996) Handbook of Optical Fibers and Cables 2nd ed. Marcel Dekker, Inc.

[16] Kuecken, John A. (1980) Fiberoptics TAB Books, Inc.

[17] Kao, C.K. (1988) Optical Fibre Peter Peregrinus Ltd.

[18] International Standard (2001) CEI IEC 60793-1-43 "Part 1-43: Measurements methods and test procedures – Numerical aperture" *International Electrotechnical Commission*, 2001-07, 1st ed.

[19] Rothrock, Larry (2002) *Personal communication*, Photran LLC..

[20] Franzen, D.L., M. Young, A.H. Cherin, E.D. Head, M.J. Hackert, K.W. Raine, and J.G.N. Baines (1989) "Numerical Aperture of Multimode Fibers by Several Methods: Resolving Differences" *Journal of Lightwave Technology* vol. 7, no. 6, 896-901

[21] www.photran.com/fiberds.htm

[22] www.crystalsystems.com/proptable.html

[23] DeWitt, D.P. and Gene D. Nutter (1988) Theory and Practice of Radiation Thermometry John Wiley and Sons, Inc.

[24] Hecht, Eugene (2002) Optics 4th ed. Addison Wesley.

Appendix A: Ray tracing

The following figures show the ray tracings performed for the theoretical/empirical evaluation section of this thesis. For a key, the color green represents the original incident ray, blue is the reflected ray, and red is the transmitted ray. This modeling is in accordance with Snell's Law and the Fresnel equations. It does not represent the "effective" value of critical angle discussed in the text. Ray tracings were prepared for incident radiation starting at -90° through +135° at increments of 15°.

-90° Incidence

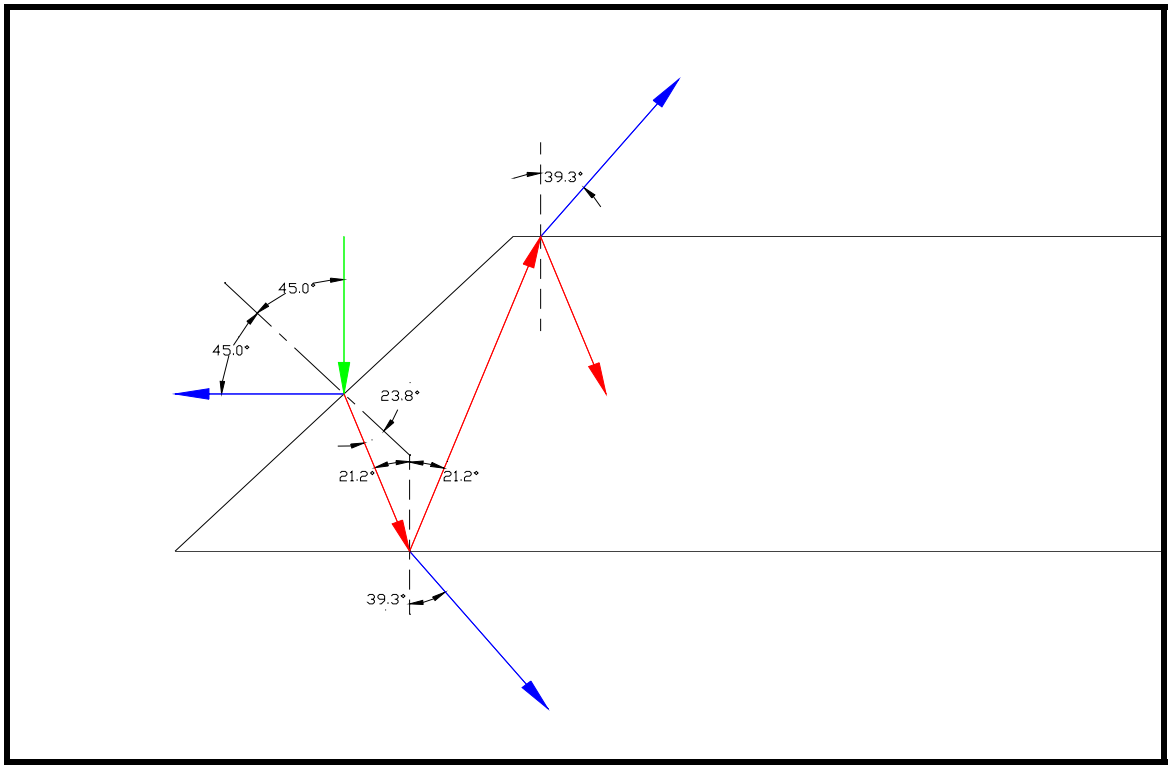

-75° Incidence

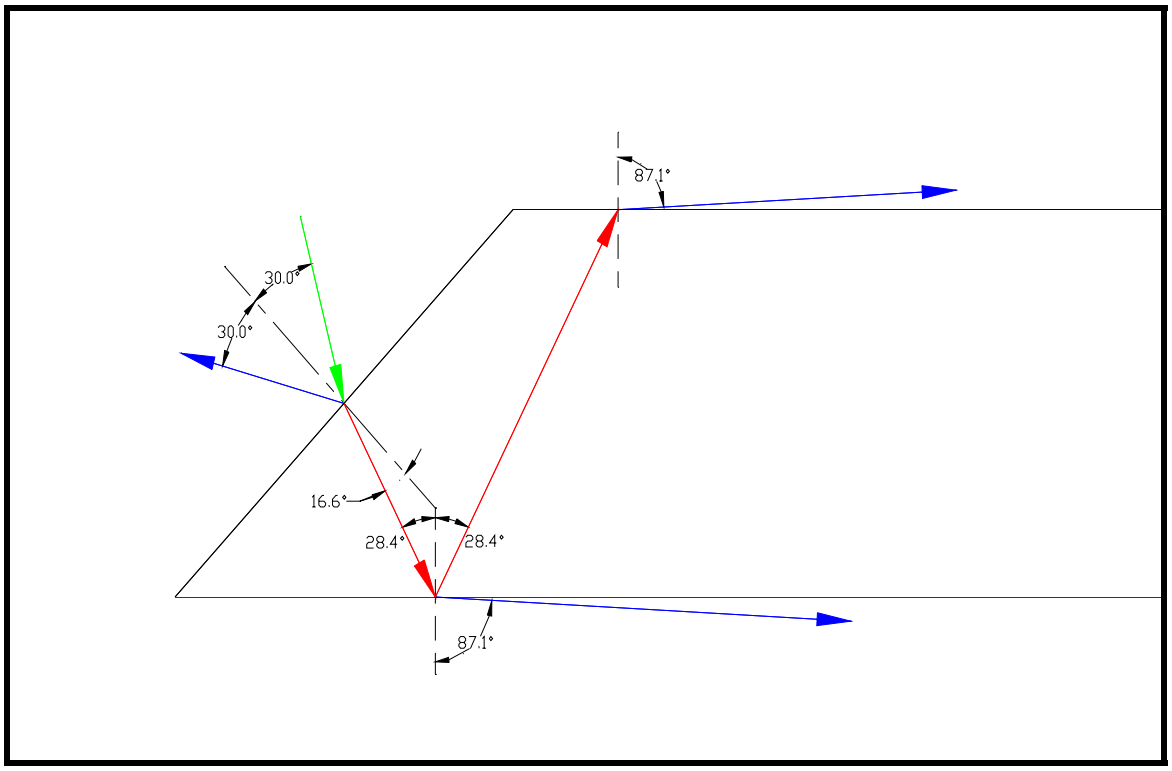

-60° Incidence

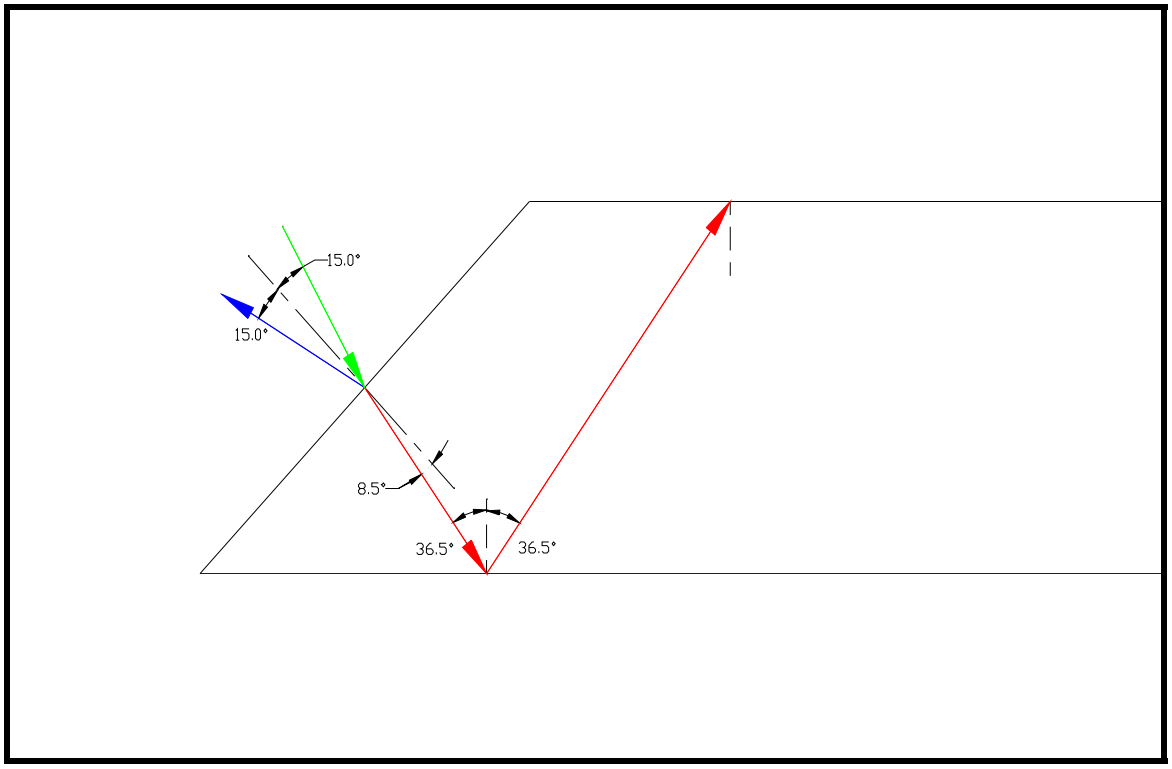

-45° Incidence

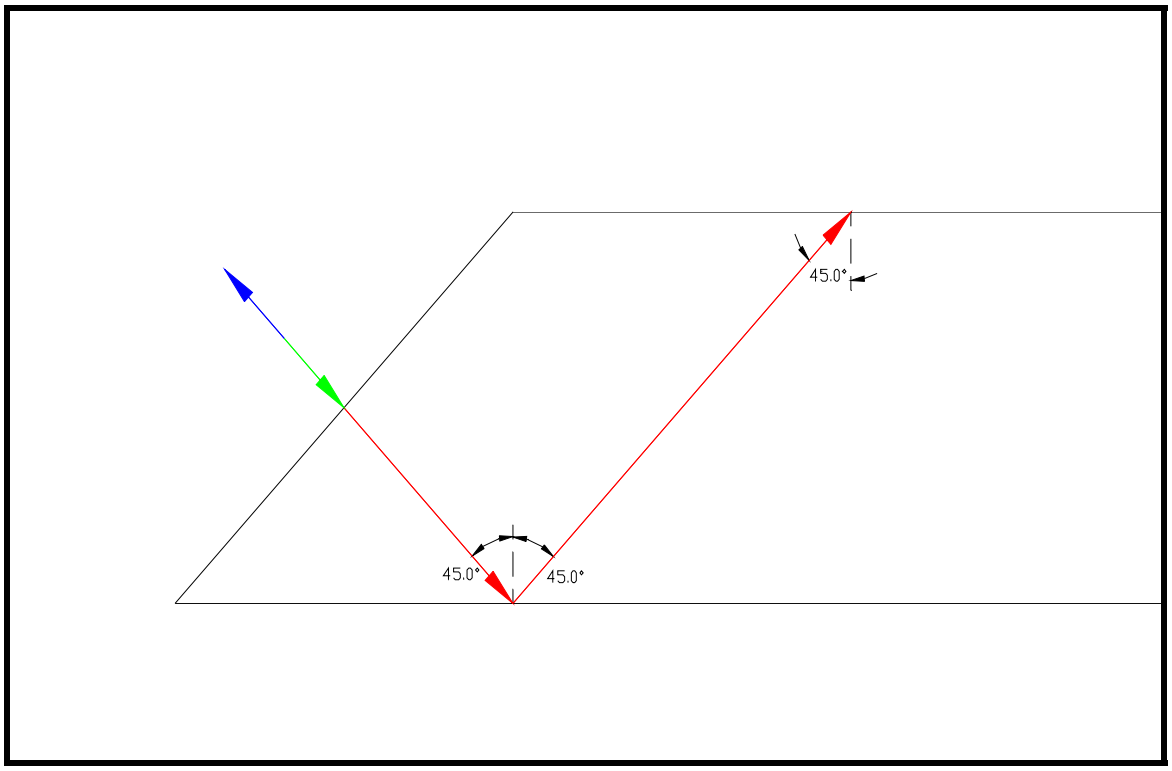

-30° Incidence

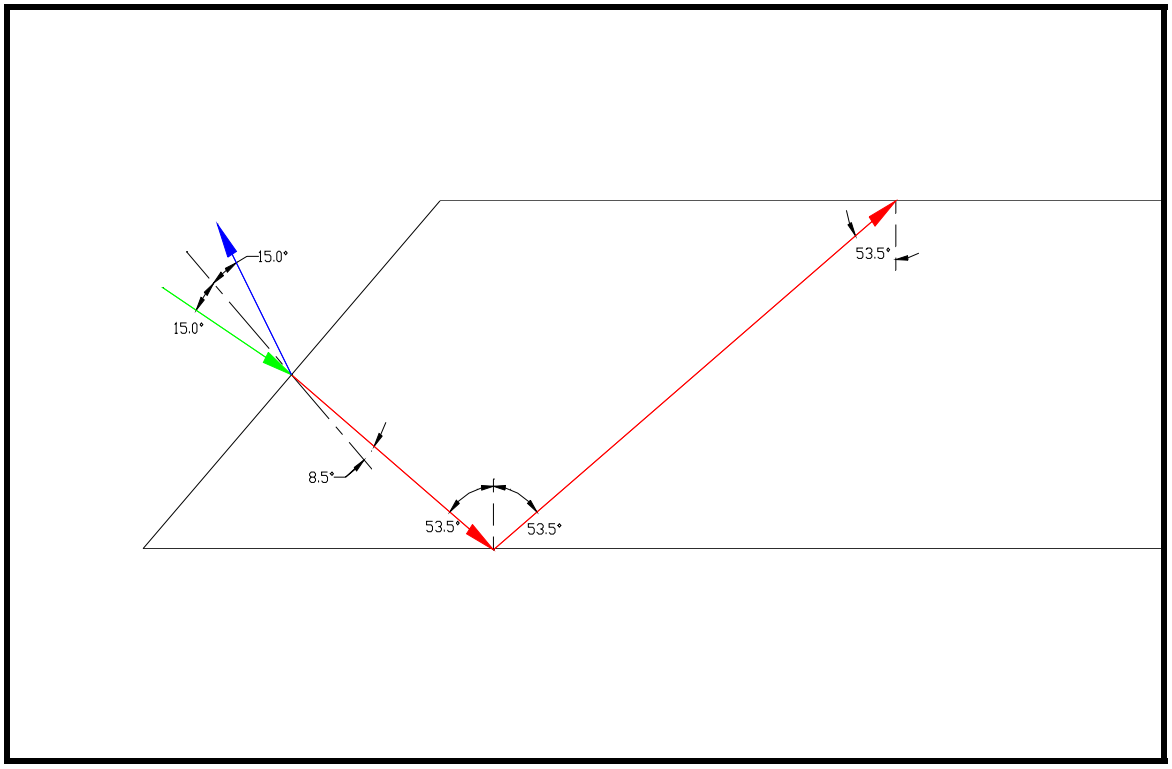

-15° Incidence

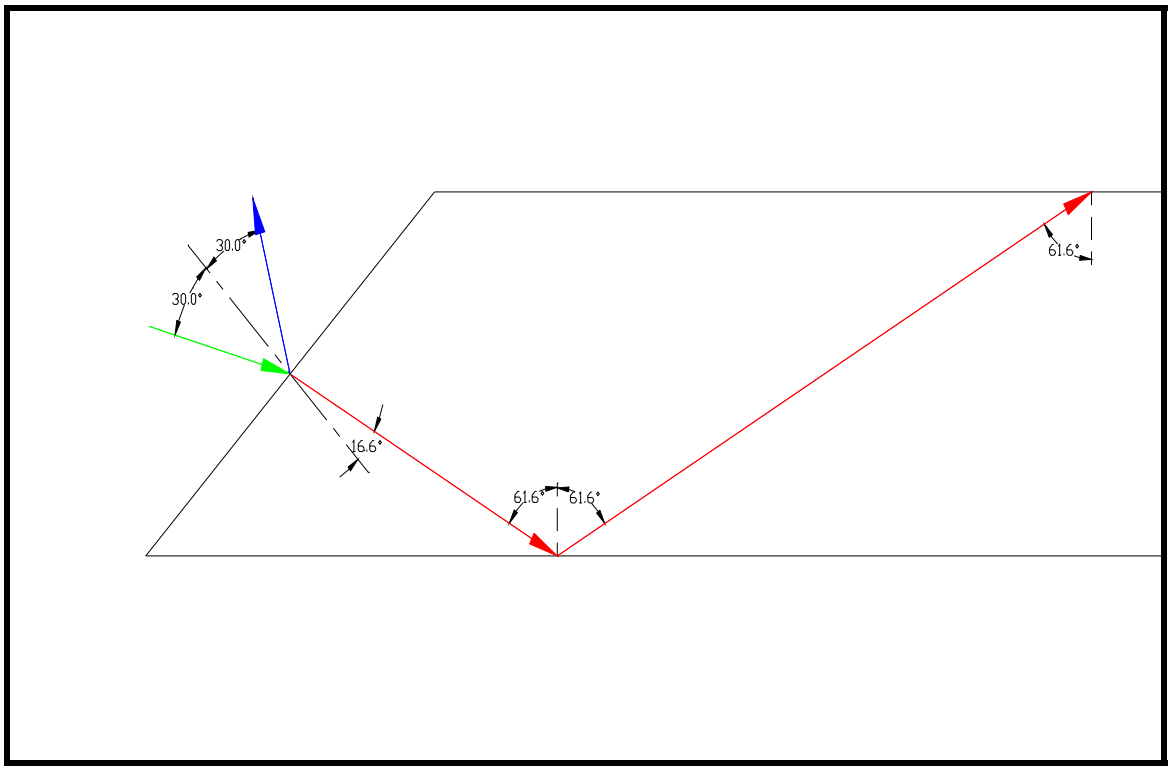

0° Incidence

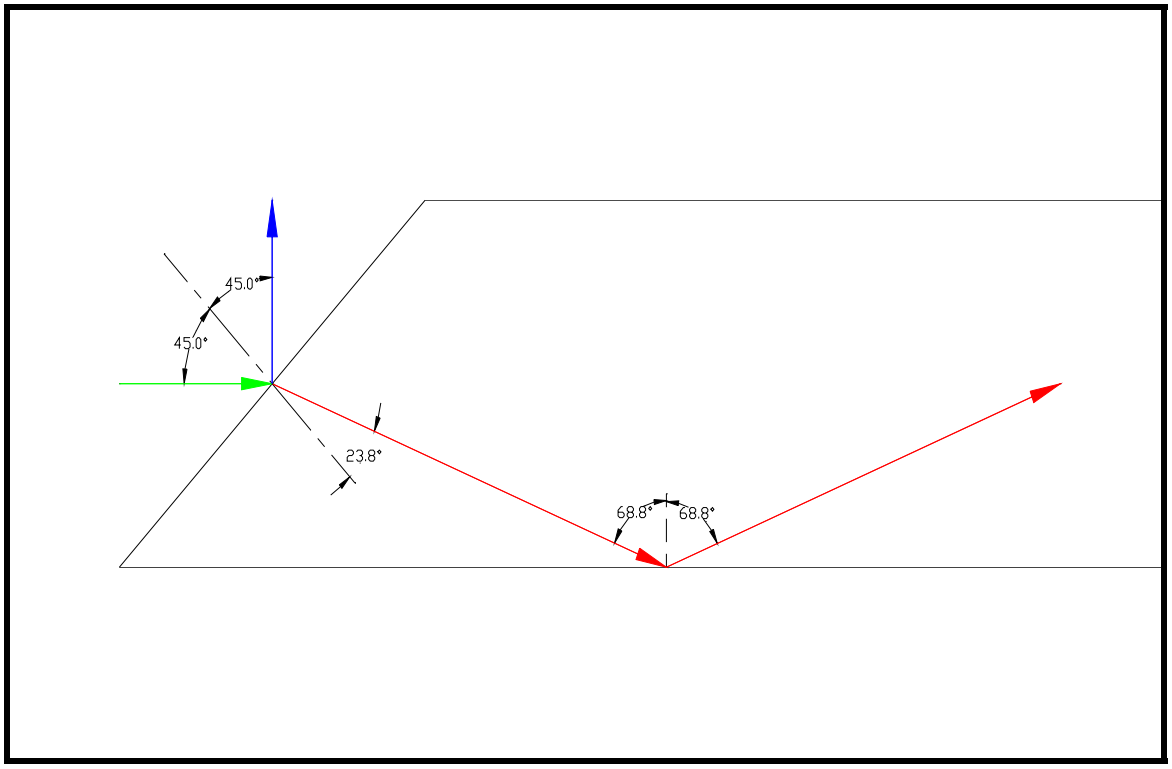

+15° Incidence

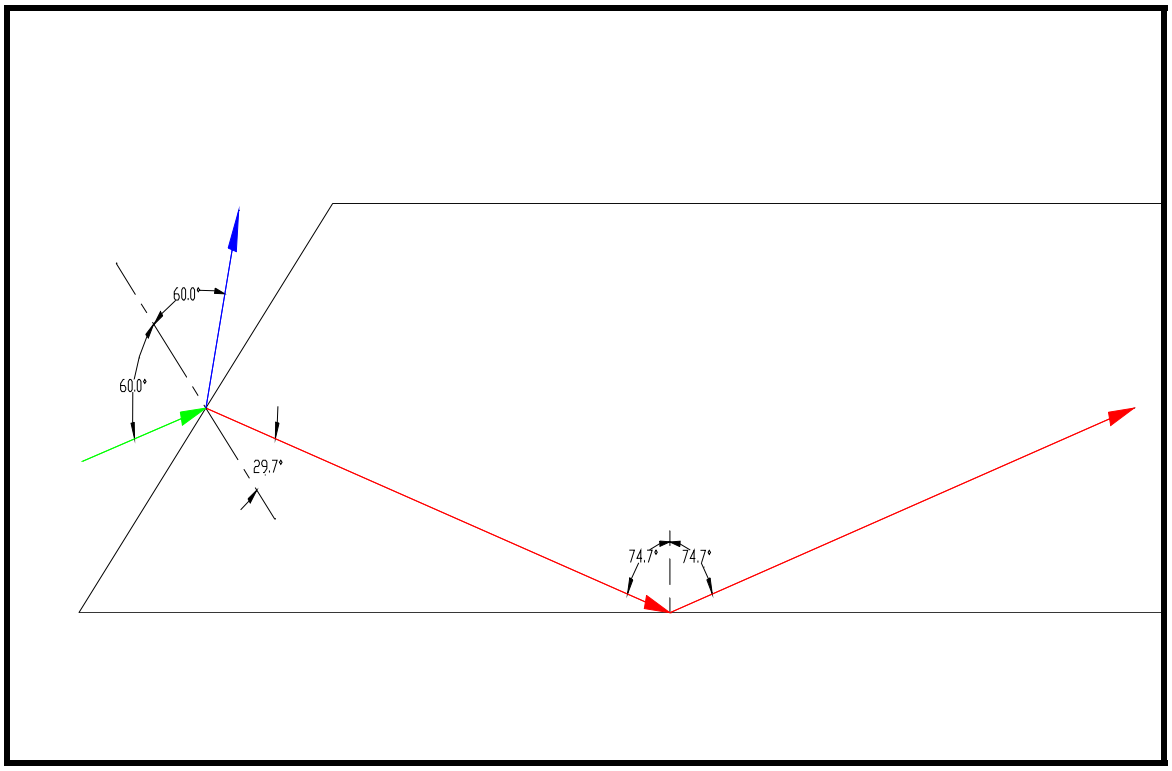

+30° Incidence

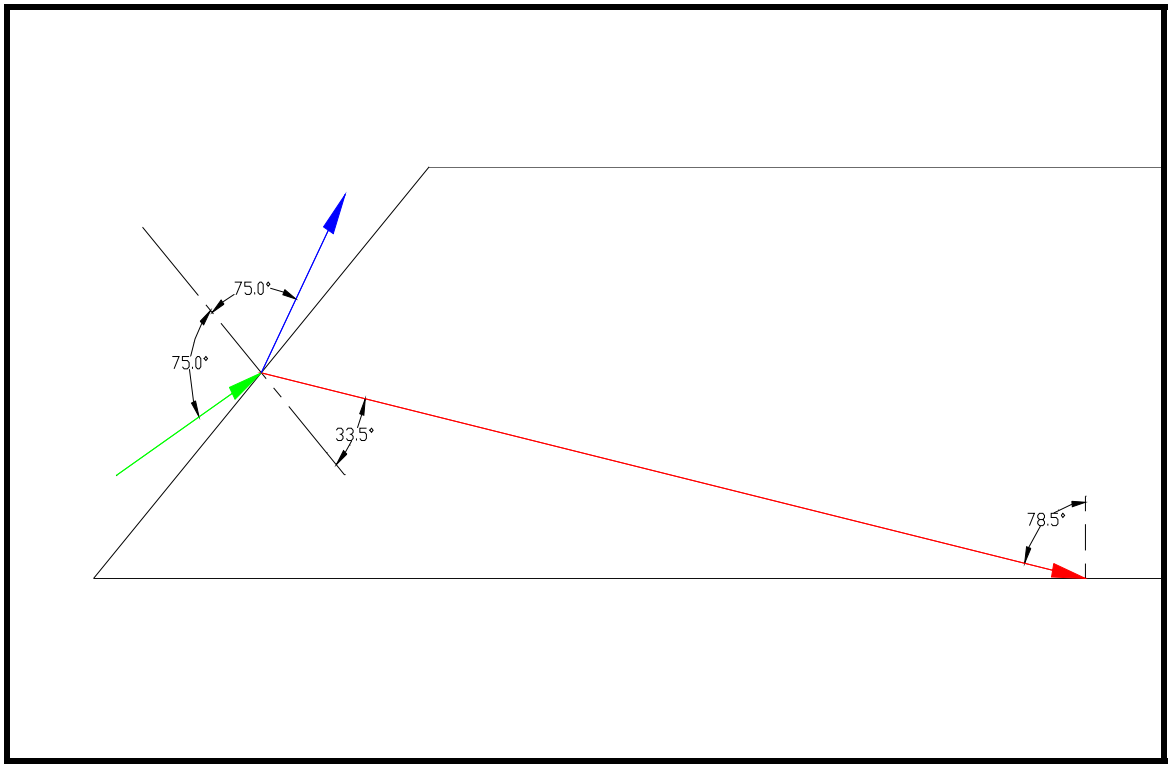

+45° Incidence

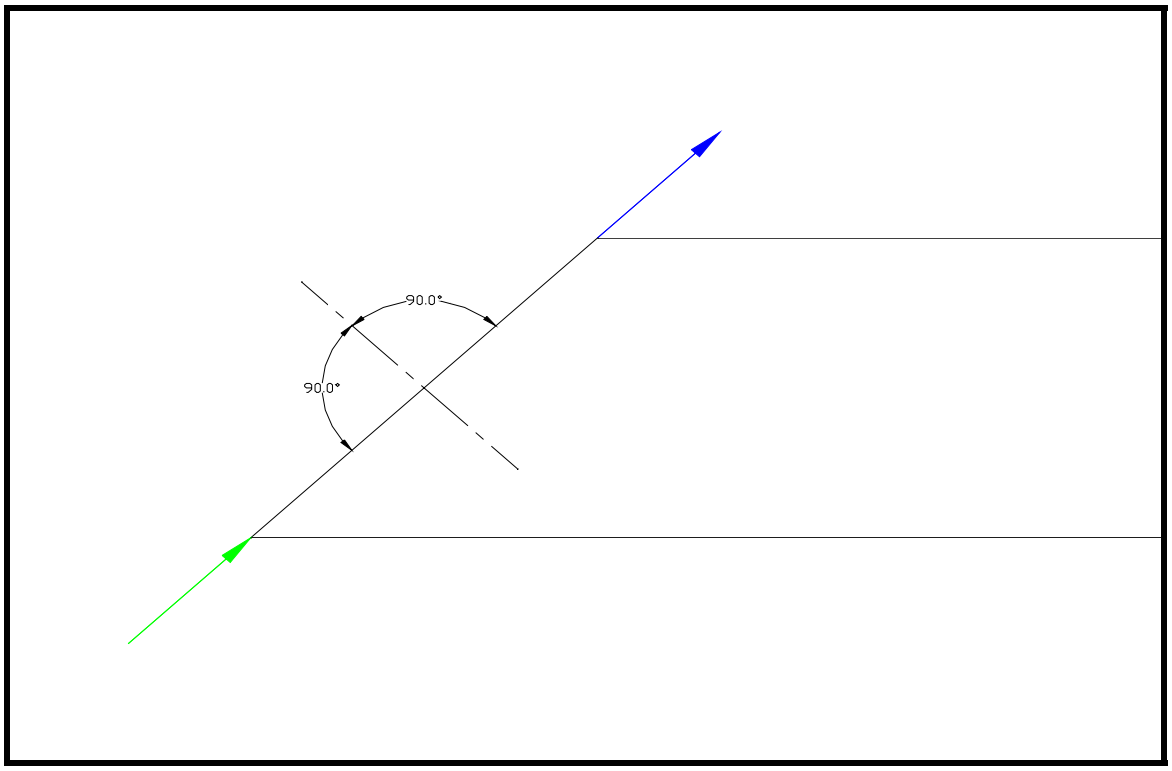

+60° Incidence

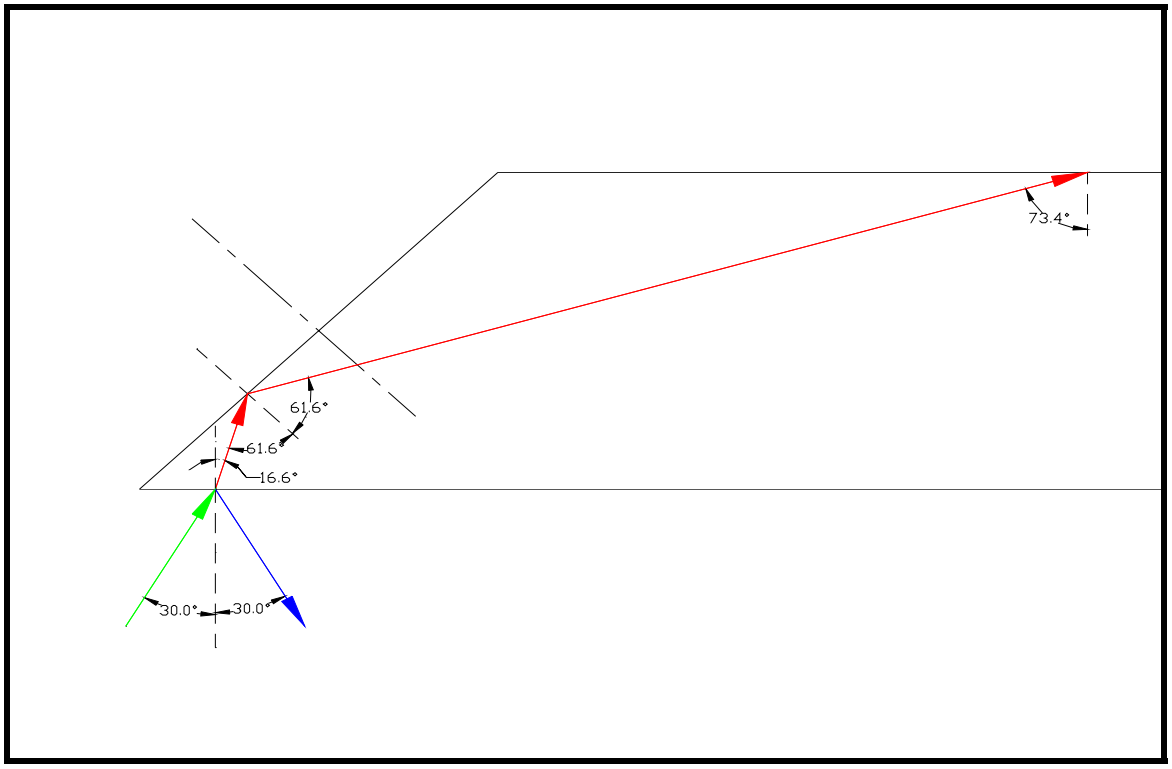

+75° Incidence

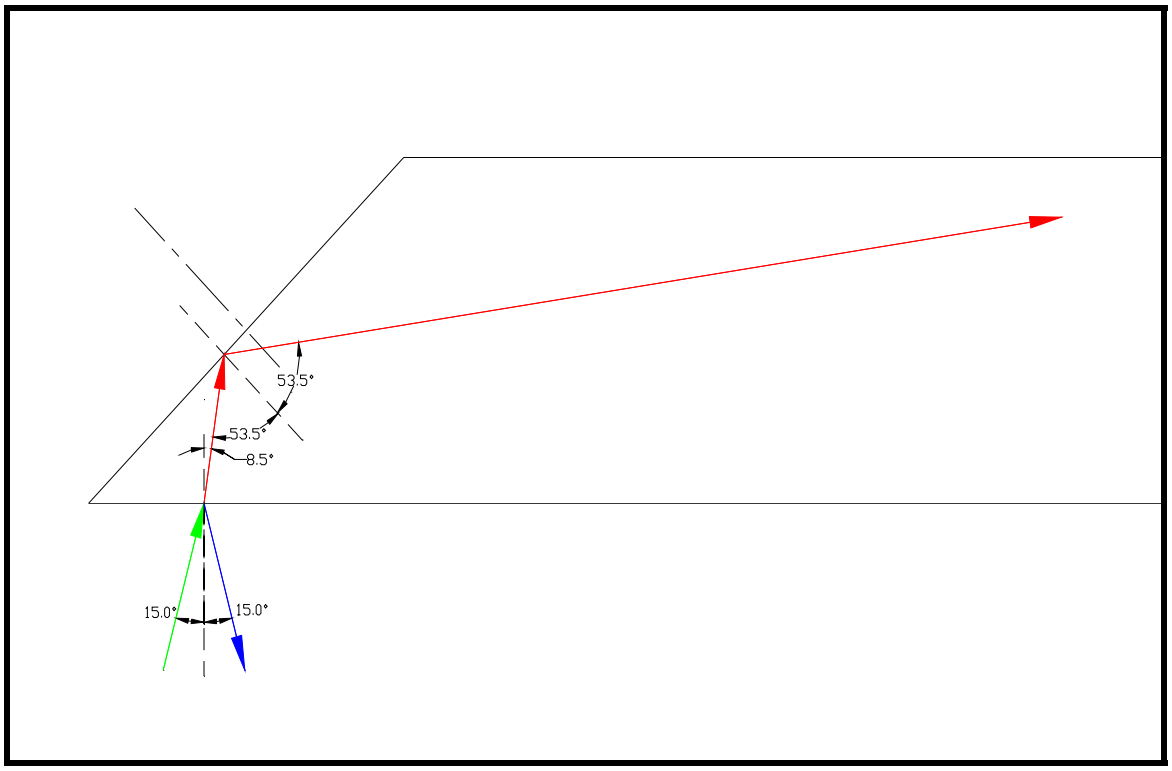

+90° Incidence

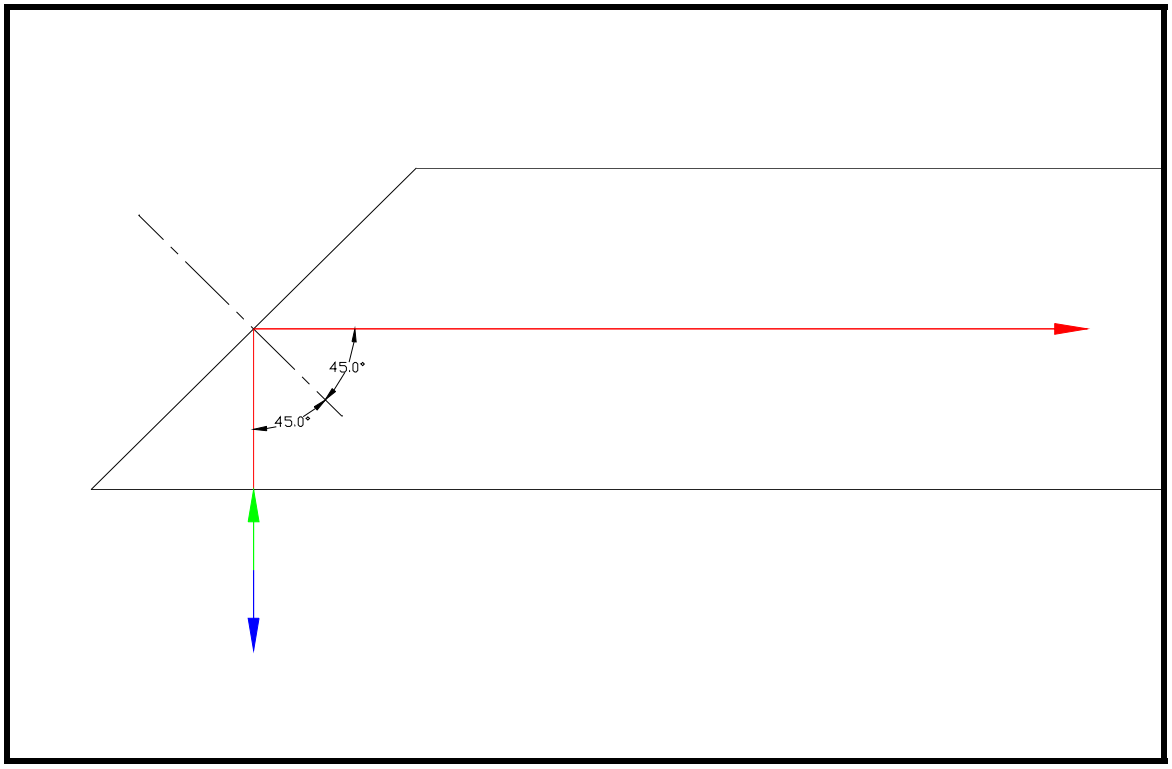

+105° Incidence

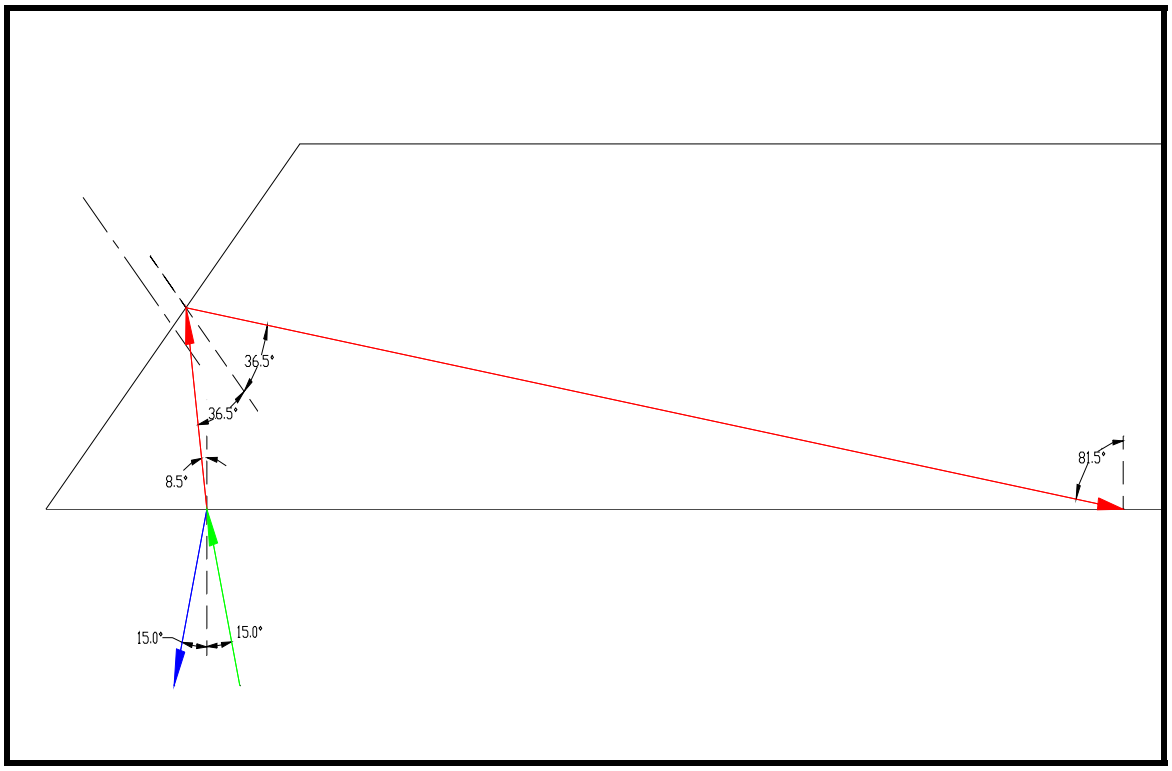

+120° Incidence

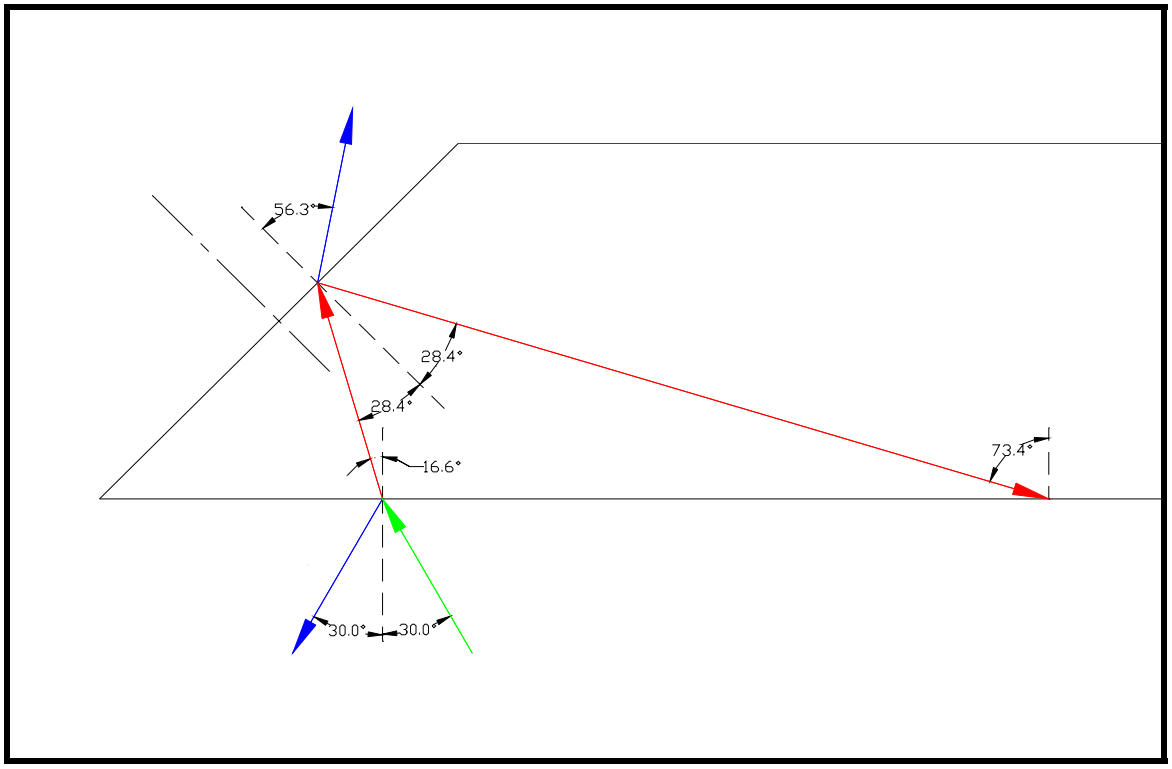

+135° Incidence